

LETTER TO EDITOR

Dear Editor,

we would like to thank you and both reviewers for the insightful comments. To answer these comments, the manuscript has changed substantially (detailed point-by-point answers to reviewers's comments are reported below). The main changes from the older version are as follows.

First, with the criticisms raised we realized there was an error in the dataset of the original manuscript (indeed, reviewer 1 was right in noting that there was a significant underestimation of OA). We do apologize for the error in the data of the original manuscript. We realized that the corrections following this mistake are substantial and significant, but the revised version shows a better consistency with the literature, in comparison with the original draft. In particular, the relation between AAEs and BC-to-OA ratios (rev. Fig.5) is now very similar to that found by both Lu et al.(2015) and Saleh et al. (2014).

Second, OA properties during the winter field campaign are now discussed in detail in [1]. In [1] we proved the correspondence between larger AAE values and larger values of an Oxygenated Organic Aerosol (OOA) component originating from biomass burning and influenced by aqueous phase processing (aqSOA). We apologize for the confusion about this point in the original manuscript. In the revised manuscript any discussion about SOA was deleted, the reader being referred to [1] for the demonstration of the correspondence between BrC and aqSOA.

Finally, to answer comments raised by both reviewers, the way aerosol size and refractive index influence BrC is analysed in detail in the revised manuscript (rev. Fig.1 and relevant text). We matched AAE measurements to numerical simulations (Mie theory) of $AAE(d_p, m, \lambda)$ resolved by particle diameter (d_p) and wavelength (λ) dependent complex refractive index ($m(\lambda)=n(\lambda)-ik(\lambda)$). BrC patterns (measured) were found to match those theoretically expected for BrC with $m(\lambda)$ taken from the literature. This consistency has allowed us to gain more strength and confidence from measurements, and to identify and characterize BrC in a clearer fashion, in comparison to the original draft.

Relevant Figures and Tables (and relevant text) have changed from the older revision as follows: (i) three figures (old Fig.1, 7 and 8) and one Table (Tab.2) deleted as requested by reviewer 2; (ii) one figure modified (older Fig.2, now Fig.1) to show measurements and simulations of AAE against aerosol size (instead of AAE vs droplet mode aerosol score); (iii) four figures (older Fig.3,4,5,6, now Fig.2,3,4,5) and one table (Tab.1) corrected (due to the error in the dataset) and slightly modified.

The review process has significantly changed (to our opinion improved) the manuscript. Relevant conclusions did not change, but are now more consistent to literature and theory. We wish this last version of the manuscript can be accepted to finalize ACP review purposes.

Sincerely yours,

Francesca Costabile (on behalf of all of the co-authors)

REFERENCES

[1] Gilardoni, S., Massoli, P., Paglione, M., Giulianelli, L., Carbone, C., Rinaldi, M., Decesari, S., Sandrini, S., Costabile, F., Gobbi, G.P., Pietrogrande, M.C., Visentin, M., Scotto, F., Fuzzi, S., Facchini, M.C.: Direct observation of aqueous secondary organic aerosol from biomass burning emissions, P. Natl. A. Sci., 113.36: 10013-10018, 2016.

AUTHOR'S ANSWERS TO REVIEWERS'S COMMENTS

We thank both reviewers for their insightful comments, and also for insisting on certain points. As already mentioned in the letter to Editor, to answer these points we realised there was an error in the original dataset. We wish to apologise for this error to both reviewers. Following correction of the error, several points shall be already answered.

Our detailed point-by-point answers to reviewer's comments are reported below (in Bold, reviewer's comments (RC); in plain text, author's answers (AA)).

1 Referee 1

RC) Looking at any of the two curves, one can see that $AAE_{BC,OA}$ increases with decreasing BC-to-OA ratio in a fashion very similar to what the authors report, simply due to the decreased contribution of BC to AAE. In other words, a constant AAE_{OA} can explain the data (whether that OA is primary or secondary does not matter). Therefore, the authors conclusion that brown aerosol is exclusively secondary OA (e.g. line 296 and line 455) does not necessarily follow from the data. The correlation with f_{44} and the droplet mode is not enough. All they can say is that aged OA contributes to the brown aerosol, but they cannot say that the brown aerosol is exclusively secondary (unless they show that all OA is secondary, which I dont think is the case).

AA) The reviewer correctly notes that this major finding does not follow from this paper. It is indeed the subject of another paper just published [1], in which we prove that the larger AAE values correspond to larger values of an Oxygenated Organic Aerosol (OOA) component originating from biomass burning and influenced by aqueous phase processing (referred to as aqSOA).

We apologize for the confusion in the original manuscript. In the revised manuscript, we explain the increase of AAE, and thus BrC formation, with the formation of secondary organic aerosol in the aqueous phase, as proved in a different paper [1]. Any discussion concerning secondary origin was deleted, the reader being referred to [1] for a complete characterization of OA properties.

RC) Now to the second major point concerning AAE_{BC} . In the previous review, I made the point that $AAE_{BC,OA}$ should converge to AAE_{BC} at large BC-to-OA ratios. This is supported by the calculations shown in Figure R1. The authors assume AAE_{BC} of 1.1 in their analysis, while their data (Figure 4 and SI Figure 1) clearly show that AAE plateaus at 1.8 at large BC-to-OA ratios. They explained this discrepancy in the revised manuscript as due to any spectrally light absorbing material that the AMS could not detect (refractory material, or material in particles smaller than 100 nm and larger than $1 \mu m$). This is not convincing. First, what is the light-absorbing refractory material with such a high AAE (it needs to be $\gg 1$ in order to have such a big influence)? It could be dust, but the authors say that they exclude data that had contribution from dust. Second, lets assume that the contribution is from OA particles that the AMS could not see (too small or too large particles). That would mean the AMS missed A LOT of OA mass. This can be explained by looking at the difference between the blue and red curves in Figure R1. The red curve is very similar to the authors data (e.g. Figure 4 in the manuscript). AAE plateaus at 1.8. If AAE_{BC} is 1.1, that would mean what the authors report as BC-to-OA = 20, should actually be 0.5 (where the dashed black line intersects the blue curve in Figure R1). Of course, this calculation is simplified, but the point is that the BC-to-OA has to be grossly underestimated (at least an order of magnitude) for the authors explanation to hold. I dont think this is the case. The more logical explanation

is that the AAE measurements, for some reason, are overestimated by $\sim 80\%$. And as I pointed out in the previous review, this would explain the unusually large $AAE_{BC,OA}$ reported in this study. I think the authors should try to address this bias, or at the very least clearly state it in the manuscript and discuss the implications.

AA) The reviewer is correct.

There was an error in the dataset. The OA-to-BC ratios corrected are more than double that uncorrected, and the BC-to-OA ratios revised are lower than 1 instead of 10 (see rev. Fig. 2, 3, and 5). Indeed the reviewer was right in noting that there was a significant underestimation of OA. We apologize for the error, and thank the reviewer for insisting on the importance of this point. After correction of the error, the relation between AAE and BC-to-OA is now far more consistent to literature than what found in the original manuscript (see revised Fig.3 and Fig.5).

RC) **Finally, it is not clear why the authors define brown aerosol as something different than brown carbon. Do they mean that there are non-organic (non-dust) components that are also brown? If yes, they need to justify. If not, it seems to me that brown aerosol and brown carbon are synonymous.**

AA) We apologize for the confusion about the ambiguous use of the term brown aerosol in the original manuscript. In the revised version we use the term brown carbon instead.

2 Referee 2

RC) 1. The discussion about the source of the brown aerosol is completely convoluted. For example, in the abstract and conclusion, the authors state it does not necessarily equate to brown carbon. However, most of the manuscript presents support for the hypothesis that this material is indeed BrC.

AA) We apologize for the confusion about the ambiguous use of the term brown aerosol in the original manuscript. In the revised version we use the term brown carbon instead.

RC) 2. The influence of the case study seems to drive a lot of the broad conclusions (for example, the trends in Figure 3). If this one day (out of 40 total included in the analysis) is removed, to the broad trends hold up? How would the values in Table 1 be different if the one day case study is removed?

AA) In the revised manuscript we clarify that the case study does not last one day, but 1.5 h, and show case study datapoints in all the relevant figures (Fig.2, 3, and 5) to illustrate how these few data relate to the broad trends (we removed accordingly panel f of Fig.5 because AAE case study data are indicated in all figures).

RC) 3. I also have some problems with the authors interpretations of their data - especially the data presented in Table 1.

AA)The reviewer is correct. We apologize for the confusion of this part of the original manuscript.

In the revised manuscript Table 1 was modified. First, we realized that there was an error in the dataset, and modified Table 1 accordingly. Then, we decided to show in Table 1 only statistically significant correlations ($p < 0.001$). In Table 2 of the supplementary material we show relevant statistical significance, i.e. the matrix of Bonferroni Probabilities (p) associated to Pearson's correlation coefficients (r).

RC) (continued) Specifically, the authors suggest that PC1, PC2 and PC4 are BC primary aerosol (line 274). The support for this statement is that all are correlated to BC and fBC, but I completely disagree with that assessment. PC2 and PC4 are not correlated at all with BC or fBC the highest R2 value is 0.04 for the correlation between PC2 and fBC. PC1 is not correlated with fBC, and is only weakly correlated with BC (R2 value is only 0.36).

AA) In the revised manuscript PCs interpretation is discussed in more detail (Par.3.3, and Par.4.1). We added numerical simulations of $AAE(d_p, n, \lambda)$ (see rev. Fig.1) to show the way PC1, PC2, and PC3 relate to theoretical values expected for BC and BrC. In addition, we showed the statistical significance of correlations (see above), and added values of correlation in the Winter and the Fall (Table 1 of the supplementary material). Finally, we decided to exclude PC4 from the analysis. PC4 is only a smaller component (approx. 8% of the variance) with loadings peaking in the nucleation mode size range (20-40 nm): as indicated by this reviewer in comment n.4, PC4 is not expected to affect significantly aerosol optical properties.

Therefore, in the revised manuscript PC1 represents the aerosol originating in the traffic rush hour in the urban area, due to local emissions enriched in OA ($r=0.9$, $p < 0.001$ in the Winter), in agreement with the literature (e.g., Costabile et al., 2009; Brines et al., 2015, and references therein). PC2 represents the nocturnal urban aerosol related to residential wood burning emissions ($r=0.4$, $p < 0.001$, with both f_{BC} and f_{OA} in the Winter).

RC) (continued) Further, line 300 claims a robust statistical relation linking AAE, this "droplet" mode component (PC3), and OA-to-BC, together with f_{OA} , $d_{med}(S)$, f_{44} and f_{43} . I do not think that Table 1 provides evidence for a robust statistical relationship, given that the highest R2 value among all the relationships analyzed was < 0.5 .

AA)As mentioned before, in the revised manuscript Tab.1 was modified. We identified statistically significant correlations (values of Bonferroni Probabilities p shown in Tab.2 of the supplementary material). These indicate that correlations linking AAE to the droplet mode aerosol ($r=0.66$ with $r=0.63$ in the Fall, $r=0.67$ in the Winter, and $p<0.001$), AAE to OA-to-BC ($r=0.78$ with $r=0.55$ in the Fall, 0.82 in the Winter, and $p<0.001$), AAE to $d_{med(S)}$ ($r=0.60$ in the Fall, 0.71 in the Winter, and $p<0.001$), and the droplet mode aerosol to OA-to-BC (0.54 , $p<0.001$) are all statistically significant correlations. In addition, in the revised manuscript the relation linking these variables is analysed in more detail through numerical simulations of $AAE(d_p, \lambda, m_\lambda)$. We show that measurements (underlying these correlations) match relevant patterns theoretically expected for BrC (rev. Par.4.1, and rev. Fig.1 and Fig.3).

With regard to f_{43} and f_{44} , we decided to delete relevant correlations from Table 1 since we proved in [1] the correspondence between larger AAE and aqSOA.

RC) 4. Building on comment 3 above, since PC3 represents larger particles compared with PC1, PC2, and PC4, it is not at all surprising that it is more strongly associated with aerosol optical properties, since it represents particles that are more optically active. This seems relevant in the data interpretation (put another way, of course PC4 has no correlation with aerosol optical properties since these particles are so small).

AA) The reviewer is right in noting that this part of the original manuscript was not clear enough.

In the revised manuscript (Par.4.1 and Fig.1) we show that AAE values increase with increasing the optically relevant aerosol size ($d_{med(S)}$), as suggested by the reviewer. As well, through numerical simulation (Mie theory) of $AAE(d_p, n, \lambda)$ expected for BrC, we demonstrate that the large AAE measured for the BrC droplet mode aerosol can be explained only by the coupling of peculiar $m_{(\lambda)}$ values and larger particle size.

This is a major finding because characterises BrC: it emphasizes that BrC properties depend on both aerosol chemical composition ($m_{(\lambda)}$) and size distribution.

RC) 5. Again, in the abstract and conclusion, it is stated that nitrate likely contributes to the aerosol absorption (lines 9 and 473). However, I see no evidence from the data to support these statements. In fact, the authors seem to acknowledge this (discussion on line 310).

AA) The reviewer is correct. As mentioned before, there was an error in the dataset. We do apologize for this error and do thank the reviewer for insisting on this point. Following its correction, aerosol fractions do change (see revised Fig.2). There is now evidence that the larger AAE values correspond to larger nitrate mass fraction. In the revised manuscript, we mentioned this correspondence suggesting that nitrate is likely associated associated with BrC particles.

RC) 6. In the abstract and conclusion, the authors claim that theirs is the first study to consider these issues. Such a claim needs to be clarified, as many prior studies have looked into secondary BrC.

AA) The reviewer is correct.

That claim was too general. In the revised manuscript, we clarified that this study provides experimental evidence that the size distribution of BrC associated with the formation of secondary aerosol is dominated by the droplet mode, consistent with recent findings pointing to the role of aqueous reactions within aerosol particles in the formation of BrC.

RC) 7. I made this same comment in the first review, but I really don't understand why the prior results from Costabile et al. (2009) have been added to Figure 1? In the text (lines 289-295), the authors suggest that this study was the only other instance in the literature where a droplet mode PC was identified from size distribution measurements. That may be because aerosol size distribution data are not routinely subjected to this PC

analysis, but the observation of a droplet mode is NOT unique to Costabile et al. (2009). Overall, Figure 1 and this discussion are quite confusing.

AA) To avoid possible confusion, Figure 1, and the associated discussion, were deleted from the revised manuscript .

RC) 8. I am still not sure how Figures 7 and 8 (and their associated discussion) add to the manuscript. If anything, these figures and discussion add confusion.

AA) To avoid possible confusion, both Figures (and their associated discussion) were removed from the revised manuscript.

RC) 9. Finally, the quality of the writing needs to be improved throughout the manuscript. There are too many grammatical corrections for this referee to itemize.

AA) A mother-tongue collaborator checked the grammatics of the revised manuscript.

Characteristics of "~~brown~~" aerosol Brown Carbon in the urban Po Valley atmosphere

F. Costabile¹, S. Gilardoni², F. Barnaba¹, A. Di Ianni¹, L. Di Liberto¹, D. Dionisi¹, M. Manigrasso³, M. Paglione², V. Poluzzi⁴, M. Rinaldi², M.C. Facchini², and G. P. Gobbi¹

¹Institute for Atmospheric Sciences and Climate (ISAC), National Research Council (CNR), Rome, Italy

²Institute for Atmospheric Sciences and Climate (ISAC), National Research Council (CNR), Bologna, Italy

³INAIL, Rome, Italy

⁴ARPA ER, Bologna, Italy

Correspondence to: F. Costabile (f.costabile@isac.cnr.it)

Abstract. We ~~characterized the nondust aerosol having the strongest spectral dependance of light absorption (as indicated by the Absorption Ångström Exponent, AAE) at visible wavelengths~~ investigate optical-microphysical-chemical properties of Brown Carbon (BrC) in the urban ambient atmosphere of the Po Valley (Bologna). ~~We defined "brown" this bulk aerosol with brown color (it does not necessarily equate to brown carbon).~~ In situ ground measurements of aerosol spectral optical properties, PM₁ chemical composition (HR-ToF-AMS), and ~~coarse and fine size distributions~~, particle size distributions were carried out in Bologna, ~~and data statistically analysed. Findings prove that "brown" aerosol is a secondary aerosol with AAE values from 2.5 to 6, containing large concentrations of organic aerosol (OA). BrC was identified through its wavelength dependence of~~ light absorption at visible wavelengths (λ), as indicated by the Absorption Ångström Exponent (AAE). We found that BrC occurs in particles with a narrow monomodal size distribution peaking in the droplet mode, enriched in nitrate and poor in BC, with a strong dependance on OA-to-BC ratios, and SSA₅₃₀ of 0.98 ± 0.01 . We demonstrate that peculiar complex refractive index values ($k_{530} = 0.017 \pm 0.001$) are necessary in addition to larger particle size to match the large AAEs measured for this BrC ($AAE_{467-660} = 3.2 \pm 0.9$ with values up to 5.3). In terms of consistency of these findings with literature, this study: (i) provides experimental evidence of the size distribution of BrC associated with the formation of secondary aerosol; (ii) contributes to sky radiometer retrieval techniques (e.g., AERONET) by adding that in the ~~larger accumulation mode particles previously referred to as droplet mode particles. Nitrate is an additional likely component. Its spectral optical signature, and possible sources, are investigated. To our knowledge, no previous work has considered these issues in the ambient atmosphere. We compared to literature to put findings in a broader perspective. There~~

is consistency with recent "diluted" urban observations (airborne, and AERONET), and combustion chamber observations. Our study adds to these previous ones that the high AAE values featuring the "brown" aerosol depend on the OA to Black Carbon (BC) ratio more than on OA, and that the link between AAE and lower troposphere AAE increases with increasing OA-to-BC (already observed for freshly emitted primary aerosols from biomass burning) does exist in the ambient atmosphere for this aged "brown" aerosol, as well. The comparison with studies on the composition evolution of OA in the atmosphere strengthens the result that this "brown" aerosol contains aged OA, and give insights into aged brown OA formation processes. Findings will have important atmospheric implications for modeling studies, ratios rather than with increasing OA; (iii) extends the dependence of AAE on BC-to-OA ratios previously observed in chamber experiments to ambient aerosol dominated by wood burning emissions. These findings are expected to bear important implications for atmospheric modeling studies and remote sensing observations, as regards parametrization and identification of brown OA, and brown carbon BrC in the atmosphere.

1 Introduction

Aerosol has an important role in the Earth's climate with both direct and indirect effects; ~~beside that~~ in addition, it affects air quality and atmospheric chemistry. At present, our understanding of the light-absorbing aerosol types is ~~very~~ incomplete (see reviews by Laskin et al., 2015; Moise et al., 2015). An important absorber of solar radiation in the visible region is ~~the~~ atmospheric carbonaceous aerosol (IPCC 2013). In the classification of its components proposed by ~~poschl2003, visible-light absorbing properties were varied~~ Pöschl (2003), visible-light-absorbing properties ranged between two extremes. On one side, there is Black Carbon (BC), refractory material that strongly absorbs light over a broad spectral range. On the other side, there is ~~the~~ colourless Organic Carbon (OC), non-refractory material, with no absorption or little absorption in the UV spectral range. There is a gradual decrease of thermochemical refractiveness and specific optical absorption going from BC graphite-like structures to non-refractive and colorless OC ~~. Also, there is a gradual decrease in the volatility from BC (the lowest volatility), to colorless non-refractory volatile OC (the highest volatility).~~ Laskin et al. (2015). A broad range of coloured organic compounds ~~, with volatility in between these two extremes,~~ have recently emerged in the scientific literature for their possible role in the Earth's ~~climate. The term "brown carbon" radiative transfer, therefore on its climate.~~

The term Brown Carbon (BrC) has emerged to describe this aerosol having an absorption spectrum smoothly increasing from the vis to the near-UV wavelengths, with a strong wavelength dependence of the light absorption coefficient ($\lambda^{-2} - \lambda^{-6}$) (Andreae and Gelencsér, 2006; Moosmüller et al., 2011; Bond et al., 2013; Laskin et al., 2015; Moise et al., 2015). BrC lacks a formal analytical definition (Bond et al., 2013). In this study, we will ~~refer to a "brown" aerosol to indicate an aerosol type with~~ identify BrC through its high values (2-6) of the visible Absorption Ångström Exponent

(AAE), a parameter describing the wavelength (λ) dependent absorption coefficient (σ_a) of light by aerosol, written as:

$$AAE(\lambda) = -\frac{d \ln(\sigma_a)}{d \ln(\lambda)}$$

60 $AAE(\lambda) = -\frac{d \ln(\sigma_a)}{d \ln(\lambda)}$ (1)

What is known about ~~the~~ BrC aerosol is that it is ~~an~~-organic matter having both primary and secondary sources (Laskin et al., 2015). Primary BrC can be emitted together with BC from low-temperature combustion processes, like wood combustion (Andreae and Gelencsér, 2006). Secondary organic aerosol (SOA) formed in the atmosphere ~~contributes to the light absorbing carbon, as~~
65 ~~well also contributes to light-absorbing-carbon~~ (Moise et al., 2015, and references therein), but only a few works have analysed the ~~secondary brown carbon~~ BrC associated to SOA (~~Saleh et al., 2013; Zhang et al., 2013, 2011~~) (~~Zhang et~~

Numerous evidences indicate increased absorption towards UV for aerosol particles ~~having high~~
~~nitrate (e.g., Zhang et al., 2013; Jacobson, 1999) and sulfate contents (Powelson et al., 2014; Lin et al., 2014; Lee et al., 2013; Song~~
~~in nitrate (e.g., Jacobson, 1999; Zhang et al., 2013) and sulfate (Lee et al., 2013; Song et al., 2013; Powelson et al., 2014; Lin et al.,~~

70 Lin et al. (2014) reported the formation of light-absorbing SOA constituents from reactive uptake of isoprene epoxydiols onto preexisting acidified sulfate seed aerosol as a potential source of secondary BrC under tropospheric conditions. Powelson et al. (2014) discussed ~~the~~ BrC formation by aqueous-phase carbonyl compound reactions with amines and ammonium sulfate. Lee et al. (2013) studied the likely ~~and unknown but uncertain~~
75 ~~effect of sulfate on the formation of light absorbing light-absorbing~~ materials and organo-nitrogen via aqueous glyoxal chemistry in aerosol particles. Song et al. (2013) observed significant light absorption at 355 and 405 nm for ~~the~~ SOA formed from an α -pinene + O₃ + NO₃ system only in the presence of highly acidic sulfate seed aerosols under dry conditions. Several studies demonstrated the importance of ammonium, both as a catalyst and as a reactant, in the formation of light-absorbing products (~~Laskin et al., 2015; Powelson et al., 2014~~) (~~Powelson et al., 2014; Laskin et al., 2015~~).

80 SOA formation can occur ~~both in in both~~ the gas and condensed ~~phase~~ phases. Recently, ~~an~~ efficient SOA production has been recognised in cloud/fog drops and water containing aerosol: water soluble products of ~~gas phase gas-phase~~ photochemical reactions may dissolve into an aerosol aqueous phase and form SOA through further oxidation, this SOA being referred to ~~as~~ "aqSOA" (Ervens et al., 2011; Laskin et al., 2015). AqSOA formation impacts total SOA mass ~~;~~ and aerosol size distributions by
85 adding mass to the so-called "droplet mode" (Ervens et al., 2011). Meng and Seinfeld (1994) showed that the aerosol "droplet mode" in urban areas is the result of activation of smaller particles to form fog, followed by aqueous-phase chemistry ~~;~~ and fog evaporation. It was demonstrated that aqSOA formation can affect aerosol optical properties by adding light-absorbing organic material at UV wavelengths (~~Shapiro et al., 2009; Ervens et al., 2011~~) (~~Shapiro et al., 2009; Ervens et al., 2011; Gilardoni et al., 2016~~).

90 ~~Very recently, Gilardoni et al. (2016) demonstrated that in the ambient atmosphere the aqSOA from biomass burning contributes to the BrC budget and exhibits light absorption wavelength dependence~~

close to the upper bound of the values observed in laboratory experiments for fresh and processed biomass-burning emissions.

Despite the efforts made, relations between optical properties and chemical composition of organic compounds with spectrally variable light absorption (high AAE) are poorly understood (Laskin et al., 2015). A number of previous works (Shinozuka et al., 2009; Russell et al., 2010; Arola et al., 2011) studied how the organic aerosol (OA) mass fraction (f_{OA}) relates to AAE, and to Single Scattering Albedo (SSA), the ratio of scattering to extinction, a key parameter ~~to understand~~ in understanding aerosol warming or cooling effect. Results from in situ measurements on the C-130 aircraft ~~mostly over Central Mexico~~ (Central Mexico) during MILAGRO (Russell et al., 2010) showed that both ~~Organics~~ organics and dust increase AAE values. Russell et al. (2010) showed a direct correlation between AAE and f_{OA} , ~~the larger particles (dust) having higher AAE, and the smaller particles (pollution related) having lower AAE.~~ On the basis of the same data, Shinozuka et al. (2009) showed that AAE generally increases as f_{OA} or SSA increases. This was explained by the presence of ~~humic-like~~ humic-like substances (HULIS) and dust, which are ~~colored~~ coloured (high AAE) ~~and~~ weak absorbers (high SSA) ~~associated~~ with high f_{OA} . ~~Very recently,~~ Saleh et al. (2014) burnt a selection of biomasses in a combustion chamber, varying the combustion parameters to obtain a range of BC-to-OA ratios. This ratio, the relative proportions of BC and OA mass, depends on fire characteristics ~~and determine~~ and on plume age, and determines its colour from black to brown to white as the ratio decreases ~~(Bellouin, 2014).~~ ~~Their.~~ Saleh et al. (2014) findings link the extent of absorbance to the BC-to-OA ratio for aged and fresh biomass burning aerosols. If confirmed ~~by further studies,~~ this link ~~can be a potentially~~ has the potential to be a strong predictive tool for light-absorbing properties of biomass burning aerosols (Bellouin, 2014; Moise et al., 2015). Following the approach of Saleh et al. (2014), Lu et al. (2015) reviewed available emission measurements of biomass burning and biofuel combustion, and found similar results indicating that AAE of the bulk OA decreases with the increasing BC-to-OA ratio. They conclude that the absorptive properties of OA from biomass/biofuel burning depend strongly on burning conditions and weakly on fuel types and atmospheric processing.

In this study, we ~~characterize the nondust aerosol having the strongest spectral dependance of light absorption (as indicated by the AAE) at visible wavelengths~~ investigate optical-microphysical-chemical properties of BrC in the ambient urban atmosphere. In situ ground ambient ~~measurements data~~ of chemical (HR-ToF-AMS), optical (3- λ nephelometer and 3- λ PSAP), and ~~micro-physical~~ microphysical (SMPS and APS) aerosol properties were taken during two field measurements in Bologna, Po Valley, ~~together with ancillary observations (including ceilometer retrievals).~~ Major features of the ~~"brown" aerosol in the ambient urban atmosphere are investigated. We used a global approach where the aerosol type, as a whole, is linked to the highest AAE values. We investigate sources of this brown aerosol.~~ BrC is identified through the AAE of the non-dust bulk aerosol. First, BrC properties are investigated (Sect.4.1) by relating AAE to ~~primary and secondary aerosol populations extracted~~

through a statistical analysis of size distribution, and mass spectral features. We then characterise physico-chemical properties of the observed brown aerosol, and illustrate a case study. Findings are then aerosol size, key aerosol types with known size distribution modality (including the droplet mode), PM₁ major chemical components (nitrate, OA, BC, sulfate, ammonium), and BC-to-OA ratios. We match patterns measured for BrC to those theoretically expected (Mie theory) for BrC in ambient aerosol to infer the λ -dependent complex refractive index. Then, we show a case study to illustrate BrC major features (Sect.4.3). Finally, findings are discussed in comparison with previous literature works literature to explore their general validity instead of treating them like results of a local study (Sect.4.4).

2 Experimental

Optical, chemical, and microphysical aerosol properties were measured, in the framework of the ARPA-ER Supersite project Supersite project funded by Emilia Romagna region, at the urban background site of Bologna (44 ° 31' 29" lat, 11° 20' 27' lon), in the Po Valley (Italy). Two measurement campaigns lasting one month were taken carried out: October 22 - November 13, 2012 (Fall campaign), and February 1-27, 2013 (Winter campaign). Measurements performed are detailed set-up are described below.

2.1 Measurement cabins and sampling lines

Equipment was set up in two different cabins, located side by side. Optical properties and coarse fraction size distributions were measured in the same cabin, all the instruments set-up set up on the same inlet system equipped with a PM₁₀ head. External In the cabin, external air was pumped in the cabin into a stainless steel tube (length = 4.0 m) by an external pump ensuring a laminar flow (Reynolds number <2000). The cabin was conditioned at kept at a temperature of 20-25°C. The difference between air temperature and dew point was enough to dry the sampled air. Chemical properties and fine and ultrafine particle number size distribution were measured through a separate stainless steel inlet tube equipped with a PM₁ head.

2.2 Optical Measurements

Spectral optical properties in the visible range were measured online with a 5-minute 5-minute time resolution. Dry aerosol absorption coefficients, $\sigma_a(\lambda)$, at three wavelengths ($\lambda = 467, 530, 660$ nm) were measured by a 3-wavelength particle soot absorption photometer (PSAP, Radiance Research), together with dry aerosol scattering coefficients ($\sigma_s(\lambda)$) at 450, 525, and 635 nm, measured by an integrating nephelometer (Ecotech, mod. Aurora 3000). Like all filter-based filter-based methods, PSAP suffers from a number of measurement artifacts, including an overestimate of absorption if light absorption is also affected by particulate light scattering, and a dependance dependence of

measurements on filter transmittance (Tr) ~~There are in literature correction algorithms developed to overcome these artifacts~~ Lack et al. (2008); Virkkula (2010); Backman et al. (2014) Bond et al. (1999), and the comprehensive review by Bond et al. (2013). ~~Lack et al. (2008); Virkkula (2010); Bond et al. (2013); Backman et al.~~

165 We corrected raw PSAP data after the iterative procedure ~~finally~~ described by Virkkula (2010), where only data with $Tr > 0.7$ were retained. The wavelength-resolved $\sigma_s(\lambda)$ necessary to correct PSAP raw data were taken from nephelometer data corrected for truncation (Anderson and Ogren (1998), Bond (2001), and Müller et al., 2011). The scattering error after the truncation error correction is $\frac{\delta(\sigma_s)}{\sigma_s} \sim \frac{\delta(\sigma_s)}{\sigma_s} = 0.02$ (Bond et al., 2013). The uncertainty of $\sigma_a(\lambda)$ derived from PSAP data after these
170 corrections has been estimated to be $\frac{\delta(\sigma_a)}{\sigma_a} \sim \frac{\delta(\sigma_a)}{\sigma_a} = 0.2$ (Virkkula, 2010; Lack et al., 2008; Bond et al., 1999; Virkkula, 2010; Cappa et al., 2008). These PSAP-derived $\sigma_a(\lambda)$ can be considered an upper limit of the "true" value (Subramanian et al., 2007; Lack et al., 2008).

After all corrections, data were checked (by visual inspection) to find any outlier/low values that could significantly influence data statistics. These values ~~can~~ could be due to variability in the measurements or to experimental errors. According to manufacturers: (i) PSAP sensitivity is $< 1 \text{ Mm}^{-1}$, and measurement range is $0-50 \text{ Mm}^{-1}$; (ii) the lower detectable limit of the nephelometer is 0.3 Mm^{-1} , with calibration tolerance of $\pm 4 \text{ Mm}^{-1}$, and measurement range $0-2000 \text{ Mm}^{-1}$. A few data (124 records having $\sigma_a < 1 \text{ Mm}^{-1}$, less than 20 records with $\sigma_s < 10 \text{ Mm}^{-1}$, and some points with $\sigma_s > 700 \text{ Mm}^{-1}$) were discarded, as they were considered dubious values (comparing to data
180 variability during the field campaigns, illustrated in the Supplementary material).

2.3 Chemical Measurements

Chemical composition of atmospheric aerosol particles were characterized online with a High Resolution Time of Flight Aerosol Mass Spectrometer (HR-ToF-AMS, Aerodyne Research Inc., Billerica) (DeCarlo et al., 2006). The HR-ToF-AMS measured the chemical composition of non-refractory
185 PM_1 (nr- PM_1), i.e sulfate, nitrate, ammonium, chloride, and organic aerosol. The instrument alternated acquisition in ~~V-mode~~ V mode (higher sensitivity and lower mass spectral resolution), and W mode (lower sensitivity and higher mass spectral resolution) every 2.5 minutes. Quantitative information discussed here corresponds to the data collected in V mode. While operating in ~~the~~ V mode, the instrument measures particle size distribution based on ~~their~~ time of flight (Jimenez et al., 2003).
190 HR-ToF-AMS data were analyzed using SQUIRRELL v1.51 and PIKA v1.10 software (D. Sueper, University of Colorado, Boulder, ~~Boulder~~, CO, USA) within Igor Pro 6.2.1 (WaveMetrics, Lake Oswego, OR). Collection efficiency was calculated according to Middlebrook et al. (2012) based on aerosol chemical composition ~~and~~ relative humidity. Data validation was performed by comparison with offline measurements of sulfate, ammonium, and nitrate concentrations in PM_1 aerosol
195 samples. The HR-ToF-AMS aerosol sample line was dried below 40% RH with a Nafion drier. The uncertainty of the AMS-derived OA was assumed to be $\frac{\delta(\text{OA})}{\text{OA}} = 0.2$ according to Quinn (2008).

2.4 Particle Number Size distributions

Particle number size distributions (PNSDs) were measured by combining a commercial Scanning Mobility Particle Sizer (SMPS, TSI mod. 3080 with Long-DMA, TSI mod. 3081, equipped with a water-based Condensation Particle Counter, CPC, TSI mod. 3787), and a commercial Aerodynamic Particle Sizer (APS, TSI). Particles from 14 nm to 750 nm of mobility diameter were sized and counted by the SMPS; particles from 0.5 to 20 μm of aerodynamic diameter were sized and counted by the APS (the procedure to fit the two PNSDs is described in ~~the~~ Sect.3.2). SMPS data were corrected for penetration errors through the sampling line, penetration efficiency due to diffusion losses (calculated according to Hinds (1999)) being higher than 98% for particles bigger than 14 nm. An impactor (nozzle of 0.457 μm) was used to remove larger particles from the SMPS sampling line.

3 Data analysis

Data measured by all the instruments were merged in a single ~~dataset of 5 minute resolution. Dataset consisted of 3211 records (1764 in fall, and 1447 in winter). The statistical analysis was done on a subset of these data with no empty field (2551 records, 5-minute time resolution dataset. This dataset includes the time series of the following variables: $\sigma_a(\lambda)$ and $\sigma_s(\lambda)$, OA, NO_3^- , SO_4^{2-} , NH_4^+ , and PNSD. Raw data were subjected to various "cleaning" processes as described in Sect.2, and then analysed as described in this section. The time series subjected to data analysis includes 11910 time points covering 40 days of measurements). These data were then cleaned, and a final dataset of 1487 records (550 in fall, and 937 in winter) was ultimately included in the statistical analysis. The longer dataset was, however, used in the analysis to evaluate single cases (e.g., (5317 time points in the Fall and 5650 time points in the case-study). Winter). This time series includes missing values. The length of the "complete" time series (i.e., with no missing value) varies from variable to variable (10897 time points for OA, 10361 time points for NO_3^- , 8999 time points for SO_4^{2-} , 9677 time points for NH_4^+ , 2656 time points for the PNSD, 2367 time points for AAE, SSA, and BC, 1820 time points for f_{BC} , f_{OA} , f_{NO_3} , f_{SO_4} , f_{NH_4} and OA-to-BC). When all the time points with at least one missing values of the variables considered are excluded, the length of the timeseries drops to approx. 1500 data points.~~

225 3.1 Inference of the optical Black Carbon mass concentration

The wavelength (λ) dependent BC absorption coefficient ($\sigma_{aBC}(\lambda)$), and equivalent BC mass concentration, were calculated using the AAE_{BC} attribution method. The measured absorption coefficient at 660 nm ($\sigma_a(660)$) was used to derive $\sigma_{aBC}(530)$, and then the BC mass concentration, assuming: (i) BC is the only light absorbing species at 600 nm, (ii) a known value of AAE_{BC} at 530-660 nm (see below), and ~~(ii)~~ iii) a BC Mass Absorption Efficiency at 530 nm to be of $10 \text{ m}^2 \text{ g}^{-1}$

(as indicated by PSAP manufacturer). In literature, $AAE_{BC}=1$ is a commonly used value for externally mixed BC; internally mixed BC is commonly assumed to have the same $AAE_{BC}=1$. In fact, AAE_{BC} for externally mixed BC ~~has been was~~ predicted to be 1 for particles with diameter < 50 ~~nm~~ nm (e.g., Bergstrom et al., 2002; Moosmüller et al., 2011), but can range from 0.8 to 1.1 for particle diameters of 50-200 nm (Gyawali et al., 2009). For ambient particles, which can be internally or externally mixed, AAE_{BC} for visible wavelengths has often been observed to be larger than 1 (Lack and Langridge, 2013; Shinozuka et al., 2009, and references therein). Theoretical calculations have shown that the AAE_{BC} for internally mixed BC can vary from 0.55 (e.g., Bahadur et al., 2012) to an upper limit of ~ 1.7 (e.g., Lack et al., 2008) depending on particle size, coating, core ~~;~~ ~~wavelengths~~ ~~and wavelength~~. In Figure 3 of the Supplementary material we show numerically simulated (Mie Theory) values of $AAE(d_p, \lambda, m)$ resolved by particle diameter (d_p) and complex refractive index ($m(\lambda)$) at visible wavelengths (λ) for BC (Sect.3.4). It is shown that the AAE of BC tends to 1 for the smaller BC particles only, and can differ significantly from 1 for the larger BC particles. Based on these ~~results and on previous~~ works, we decided to use $AAE_{BC}=1.1$. The uncertainty $\delta(AAE_{BC})$ was set to $\frac{\delta(AAE_{BC})}{AAE_{BC}} 22\%$ ($\frac{\delta(AAE_{BC})}{AAE_{BC}}=0.22$ (Lack and Langridge, 2013)) according to Lack and Langridge (2013). BC uncertainty ($\delta(BC)$) was derived propagating this $\delta(AAE_{BC})$ together with the uncertainty of PSAP-derived σ_a (see Sect.2.2).

We discarded data possibly affected by desert dust (43 records over 5 days of measurements) to ensure that the equivalent BC mass concentration is not affected ~~from contamination~~ by desert dust ~~contamination (assumption i above)~~. Dust-free aerosol conditions were identified based on the analysis of aerosol spectral optical properties, increasingly applied to gather information on aerosol type (e.g., Bergstrom et al., 2007; Clarke et al., 2007; Yang et al., 2009; Russell et al., 2010; Gyawali et al., 2012; Lee et al., 2012; Costabile et al., 2013). We (e.g., Bergstrom et al., 2002; Shinozuka et al., 2009; Russell et al., 2010; Arola et al., 2012) ~~in particular, we~~ followed the methodology proposed by Costabile et al. (2013) ~~(further discussed in Sect.5.2). Accordingly, which identifies~~ the aerosol dominated by dust ~~shows this by a~~ distinctive combination of scattering ~~and~~ absorption Ångström Exponents (SAE, AAE) ~~and~~ Single Scattering Albedo (SSA) spectral variation (dSSA): ~~SSA₅₃₀ > 0.85, SAE₄₆₇₋₆₆₀ < 0.5, AAE₄₆₇₋₆₆₀ ~ 2, dSSA₆₆₀₋₄₆₇ = 0.05-0.3~~. Data points of the time series fulfilling ~~all these conditions together this distinctive combination (indicated in Table 3 of the Costabile et al. (2013) 's paper)~~ were excluded from the analysis.

3.2 Fitting procedure for the particle number size distribution

~~Data of particle~~ Particle number size distributions (PNSDs) were measured by two different instruments (SMPS and APS, Sect.2). These data were merged to obtain one PNSD based on particle electrical mobility diameters (d_m) ranging from 14 nm to 14 μ m. PNSDs measured by APS are

265 based on aerodynamic diameters (d_a); these data were converted to PNSDs based on d_m according to Eq.2 (Khlystov et al., 2004; Seinfeld and Pandis, 2006):

$$d_m = \chi \frac{C_c(d_m)}{C_c(d_a)} \frac{d_a}{(\frac{\rho_p}{\rho_0 \chi})^{1/2}} \quad (2)$$

where χ is the shape factor, $C_c(d_m)$ and $C_c(d_a)$ are the slip correction factors based on d_m and d_a respectively, ρ_p is the particle density, and ρ_0 is the unit density ($1 \text{ g}\cdot\text{cm}^{-3}$). In applying Eq.2
270 to convert APS data, we assumed: ~~particle diameter (d_p) = d_m~~ represents the true particle diameter; $C_c(d_m) = 1$ and $C_c(d_a) = 1$ (continuum regime); $\chi = 1$ (spherical particles); ρ_p continuously varying from 1.6 to $2 \text{ g}\cdot\text{cm}^{-3}$.

Particle Number Size Distributions PNSDs (i.e., $n_N(\log_{10}d_m) = \frac{dN}{d\log_{10}(d_m)}$) measured by SMPS and APS (PNSD_{SMPS}, PNSD_{APS}) overlap for d_m ranging from 460 nm to 593 nm. In this size
275 range, PNSD_{SMPS} and PNSD_{APS} were replaced by PNSD_{fitted}. PNSD_{fitted} was assumed to vary according to a power-law function (Junge size distribution) (Khlystov et al., 2004; Seinfeld and Pandis, 2006) (Eq.3):

$$n_N(\log_{10}d_m) = \frac{c}{d_m^\alpha}, \quad (3)$$

The coefficients c and α were calculated by an iterative procedure: (i) c was randomly initialized
280 from 0 to 1000; (ii) α was calculated by Eq.3 constraining values from 2 to 5, as typically found for atmospheric aerosols (Seinfeld and Pandis, 2006). PNSD_{fitted} replaced PNSD_{APS} and PNSD_{SMPS} when their relative difference (~~$d_r\delta(\text{PNSD})$~~ , Eq.4):

$$\underline{d_r\delta(\text{PNSD})} = \frac{|PNSD_{SMPS} - PNSD_{APS}|}{\max[PNSD_{SMPS}, PNSD_{APS}]} \quad (4)$$

was larger than 0.1 cm^{-3} . This procedure was considered acceptable if: (i) the minimum mean
285 squared error between PNSD_{fitted} and PNSD_{APS} was less than 1%; (ii) correlation coefficients between PNSD_{fitted} and PNSD_{SMPS}, and between PNSD_{fitted} and PNSD_{APS} were larger than 0.8. ~~A number of (98 of the~~ records did not verify these conditions, and were checked by visual inspection: 94 of them were discarded, and 4 accepted). The final dataset contained PNSD data based on d_m from 14.1 to 429.4 nm measured by the SMPS, from 446.1 to 699 nm generated by
290 the fitting procedure, and from 0.7 to $14 \mu\text{m}$ measured by the APS. The Particle Surface Size Distribution (PSSD, i.e. $n_S(\log_{10}d_m) = \frac{dS}{d\log_{10}(d_m)}$) and Particle Volume Size Distribution (PVSD, i.e. $n_V(\log_{10}d_m) = \frac{dV}{d\log_{10}(d_m)}$) were calculated from this PNSD under the hypotheses of spherical particles (Hinds, 1999; Seinfeld and Pandis, 2006).

3.3 Principal component analysis of PNSD

295 PNSDs were statistically analysed through Principal Component Analysis (PCA) .PCA was calculated
following the findings of a previous long-term study over multiple sites (8 concurrent stations)
to identify key aerosol types with known modality. The relevant methodology was described in a
previous study by Costabile et al. (2009). Four principal components (PC1-PC4) were extracted,
explaining 90of the variance. We interpreted these PCs based on: (i) their statistical properties, i.e.
300 "scores" and "loadings" (loadings indicate correlations between PNSDs and PCs, i.e. the "mode" of
the PNSD associated to the PC); (ii) Pearson's correlation coefficients (r) shown in Table 1, between
PCs, AAE, and PM₁ mass fractions of BC, organics, nitrate, sulfate, and ammonium (f_{BC}, f_{OA},
f_{NO₃}, f_{SO₄}, f_{NH₄}). The median diameter of the particle surface size distribution (d_{med(S)}) in Table 1
is intended to add information on optically relevant aerosol sizes. The OA to BC ratio (OA to BC) in
305 Table 1 is intended to indicate both combustion characteristics (higher for biofuels than for fossil fuel
combustion), and aerosol ageing (lower for fresh aerosols) (Saleh et al., 2014; Bond et al., 2013).
Correlations to f₄₃ and f₄₄ (defined as the ratio of the AMS signal at m/z 43 and m/z 44, respectively,
to the total organics AMS signal) in Table 1 are intended to add information on the oxidised OA.
The higher the f₄₄, the more oxidised the OA; the higher the f₄₄/f₄₃ ratio, the lower the volatility of
310 this oxidised OA (Moise et al., 2015).

Statistical properties used to interpret PC are "scores" and "loadings". PCs In short, Principal
Components (PCs) retained in the analysis were arranged in decreasing order of variance explained
(λ_k , called eigenvalue of PC_k), PC1 being the component explaining the largest λ_k . The k^{th} eigen-
vector is composed of scalar coefficients describing the new PC_k as a linear combination of the orig-
315 inal variables (the original variables are the time series of dN/dlog(d_p)). Coefficient Factor loadings
of PC_k represent the relative weight (in terms of correlation) of dN/dlog(d_p) variables in of the
original variables in the PC_k .Factor loadings of PC_k represent these coefficients scaled re-scaled
by the λ_k explained by the PC_k. Loadings of PC_k thus represent the relative weight of dN/dlog(d_p)
variables in PC_k thus show the "mode" of the PNSD associated to the PCs. Factor scores of PC_k
320 are the transformed variables corresponding to a particular data point in the represent the time series
of the dN/dlog(d_p) variables. Factor scores PC_k values in the new coordinates of the space defined
by the PCs. Scores thus represent the PC_k values corresponding to each particular data point of the
dN/dlog(d_p) time series in the time series of the original variables.

Weekly diurnal cycles, and loadings of PC1-4 PCA retained three principal components (PC1-PC3)
325 explaining approximately 80% of the variance. Factor loadings and diurnal cycles of scores for
PC1-PC3 are illustrated in supplementary material. PC1, PC2, and PC4 are BC primary aerosol
(all correlated to BC and f_{BC}). PC1 and PC4 are both sourced by traffic emissions, diurnal cycles
peaking at rush hours and week days. Figure 2 of the supplementary material, while Pearson's
correlation coefficients r between these PCs and the other variables measured are shown in Table
330 1. Table 1 and Table 2 of the supplementary material show relevant r values in the Winter and in

the Fall, and relevant Bonferroni adjusted probabilities (p values), respectively. These PCs were interpreted as follows:

PC1 is a fine mode aerosol component (the PNSD mode peaking from 100 to 200 nm), PC4 an ultrafine aerosol component (PNSD peaking from 20 to 40 nm). PC2 is an ultrafine BC aerosol component, as PC4. Unlike PC4, however, PC2 higher scores are at night-time, and there is no weekly cycle and no peak at "rush hours": PC2 is probably sourced by heating emissions the largest component in terms of variance explained (51 %). Loadings peak in the 80-300 nm size range. Factor scores correlate to OA and BC. Weekly diurnal cycles of these scores are higher on working days and in the road-traffic rush hour. This PC represents the aerosol enriched in OA originating in the traffic rush hour in the urban area, due to local emissions (e.g., Costabile et al., 2009; Brines et al., 2015, and references therein).

The remaining PC3 (more than 10PC2 explains 14 % of the variance. Loadings peak in the ultrafine size range (approx. 100 nm). Factor scores show diurnal cycles higher at night and in the Winter, with a slightly larger contribution during the week-ends. It correlates (inversely) to aerosol size and (directly) relates to a secondary aerosol. It is the only PC inversely correlated to f_{BC} , and directly correlated to f_{OA} , f_{AA} , OA-to-BC, and $d_{med(S)}$, with higher scores at daytime and during week days, the PNSD peaking in the accumulation mode (supplementary; in the Winter it correlates to both f_{OA} and f_{BC} (0.40, $p < 0.001$, Tab.1 of the Supplementary material). To enhance the interpretation of the aerosol type represented by this PC, Fig. ?? shows its factor loadings (brown line) in comparison to those of a PC from a previous study (Costabile et al., 2009), which has very similar statistical properties. This PC should represent the nocturnal urban aerosol related to residential heating emissions.

PC3 explains 13% of the variance. Loadings peak in the larger accumulation mode size range (from 0.3 to 1 μm). Diurnal cycles of scores are higher in daytime. It is inversely correlated to f_{BC} , and directly to nitrate, sulfate and ammonium. This PC was found to represent represents the droplet mode aerosol. The droplet mode is a submode of the accumulation mode, resulting poor in BC previously found to originate in the wet aerosol from the activation of condensation mode particles to form cloud/fog drops, followed by aqueous-phase chemistry, and droplet evaporation (John, 1990; Meng and Seinfeld, 1994; Seinfeld and Pandis, 2006; Ervens et al., 2011). To our knowledge, the work by Costabile et al. (2009) is the only work in literature showing a similar PC to compare with: authors based its interpretation on five PCAs calculated on a two year dataset over eight concurrent measurement sites, correlated to meteorological and air quality data (green, blue, red,

3.4 Numerical simulations of AAE

Values of $AAE(d_p, \lambda, m)$ resolved by diameter d_p , radiation wavelength (λ), and complex refractive index ($m(\lambda) = n(\lambda) - ik(\lambda)$), were numerically simulated according to Mie theory (e.g., Bohren and Huffman, 1983; Moosmüller et al.). The aim was to reproduce patterns expected for BrC, BC and the urban background aerosol impacted

by biomass burning emissions, as these were abundant in the study area. Simulations are illustrated in Figure 3 of the supplementary material, the relevant methodology being described in a previous study by Costabile et al. (2013).

370 To simulate patterns expected for BrC in the urban ambient aerosol, we used λ dependent complex values of $m_{(\lambda)}$ inferred during CAPMEX for an air mass with $AAE_{405-532}=3.8$ (standard deviation=3.4), characterised by high Organic Carbon (OC) to sulfate (SO_4^{2-}) ratio and high nitrate (NO_3^-) to SO_4^{2-} ratio (Flowers et al., 2010; Moise et al., 2015). These are $m_{467}=1.492-0.026i$, $m_{530}=1.492-0.017i$, $m_{660}=1.492-0.014i$, the uncertainty for $n_{(\lambda)}$ and $k_{(\lambda)}$ being set to ± 0.01 and black lines in Fig.1
375 indicate the droplet mode PC identified by these five PCAs, calculated by varying the dataset time length and number of measurement sites). The broad similarities between this PC and PC3 allow to deduce with a reasonable statistical accuracy that PC3 does represent the droplet mode aerosol ± 0.001 , respectively.

To simulate patterns expected for BC we used λ independent complex values of m estimated by
380 Alexander et al. (2008) for soot carbon particles at 550 nm: $n=1.95-0.79i$ at $\lambda=467$, as well. This comparison ultimately demonstrates that the "brown" aerosol is secondary in origin (the droplet mode is secondary in origin, because formed through secondary processes in the atmosphere (John, 1990; Meng and Seinfeld, 1994)).
nm. Note in Fig. 2 of the supplementary material the resulting variability with d_p of $AAE_{467-660}$ for BC: values of $AAE=1$ correspond only to $d_p \ll 100$ nm.

385 To simulate patterns expected for the urban background aerosol impacted by biomass burning emissions we used values of $m_{(\lambda)}$ inferred in a previous study for the smaller accumulation mode particles enriched in BC from biomass burning smoke (Costabile et al., 2013): $m_{467}=1.512-0.027i$, $m_{530}=1.510-0.021i$, $m_{660}=1.511-0.022i$, the uncertainty for $n_{(\lambda)}$ and $k_{(\lambda)}$ being set to ± 0.01 and ± 0.001 , respectively.

390 4 Results and discussion

In this section, we first identify a "brown" aerosol (AAE from 2 to 6) by relating AAE to key aerosol populations extracted through a combined statistical analysis of PNSD, and organic aerosol mass spectra. We then characterise physico-chemical properties of the observed "brown" aerosol as regards number and mass size distribution (and relevant modes), and major PM_{10} chemical components (BC,
395 organics, nitrate, ammonium, and sulfate), relevant mass fractions, and ratios. A case study is finally illustrated.

4 Results and discussion

In this section we first identify brown carbon (BrC) and characterize its optical-microphysical-chemical properties (Sect.4.1), then illustrate a case study (Sect.4.2), and finally discuss findings in comparison
400 to literature (Sect.4.3).

4.1 "Brown" aerosol: identification and features

Key aerosol types were identified through a statistical approach. PNSD principal components (PCs) were identified by

4.1 Brown carbon: identification and features

405 Several literature studies identify BrC based on its high AAE values, i.e. from 2 to 6 (e.g., Andreae and Gelencsér, 2006; Bond et al.,
At a certain range of wavelengths (λ), these high AAE values in the bulk aerosol depend on several
factors, including aerosol size, chemical composition, and aerosol mixing state. To analyse the
AAE dependence on aerosol size we used two different approaches. First, we calculated $d_{med(S)}$,
i.e. the median mobility diameter of the particle surface size distribution (PSSD, Sect.3.2). The
410 $d_{med(S)}$ is intended to represent the optically relevant aerosol size representative of the entire particle
population. Second, we analysed the aerosol population particle number size distribution (PNSD)
to find major aerosol types (i.e., Principal Components, PCs), as described in detail in Sect.3.3.
Two components (PC1 and PC2) were related to smaller particles originating from local emissions
(road-traffic and residential heating, respectively), and one component (PC3) was related to larger
415 particles (droplet mode) originating from the aerosol processing. Statistically significant Pearson's
correlation coefficients (r) between these PCs, AAE, $d_{med(S)}$ and PM_{10} major constituents are shown
in Tab. 1. The Supplementary material show relevant r values observed in the Winter and in the
Fall (Tab.1), and gives insights into its likely formation process. This conclusion is reinforced by
the correlation with f_{44} (Tab. 1) the matrix of Bonferroni Probabilities (p) associated to these r values
420 (Tab.2).

In Table 1, it is indicated a robust statistical relation linking AAE, this "droplet" mode component
The AAE correlates well with the $d_{med(S)}$ ($r=0.60$, $p<0.001$). Figure 1 shows that the measured AAE
increases with increasing $d_{med(S)}$ of the aerosol population (grey markers). In addition, markers in
Fig. 1 show the AAE and $d_{med(S)}$ representative of aerosol dominated by traffic emissions (PC1),
425 wood burning emissions (PC2), and droplet mode particles (PC3). To interpret these measurements,
we show patterns theoretically expected, based on the Mie theory, for BrC in the ambient aerosol
(brown line), a pure BC particle (black line), and an urban background aerosol impacted by wood
burning emissions (grey line). These simulations, including relevant values of the complex refractive
index $m(\lambda)=n(\lambda)-ik(\lambda)$, are described in detail in Sect.3.4. The lowest AAEs measured during
430 this study tend to values expected for pure BC, and are similar to values calculated for the urban
background aerosol impacted by wood burning emissions. Both aerosol types which were related to
local emissions (PC1 and OA-to-BC, together with f_{OA} , $d_{med(S)}$, f_{44} and f_{43} . Figure ?? shows this
relation. When PC2) match these patterns. Larger AAEs (3.2 ± 0.9) correspond to the droplet mode
PC-scores positive (PC scores >0 indicate that this aerosol type forms), the aerosol (PC3), and are
435 similar to the AAE expected for Brown Carbon aerosol. Fig.1 suggests that the threshold value of

AAE₄₆₇₋₆₆₀ distinguishing BrC is AAE is greater than 2.5. Both AAE and droplet mode increase with increasing OA-to-BC, and f_{44} , both indicators of OA aged in the atmosphere (Bond et al., 2013). Data, therefore, identify a "brown" aerosol type, >2.3 . The dotted black line in Fig.1 shows the increase of the AAE measured with increasing $d_{med(S)}$; brown and grey lines show the increase of the AAE theoretically expected with increasing aerosol size, $m(\lambda)$ being constant. Comparing these three lines, it is evident that peculiar values of $m(\lambda)$ are necessary in addition to the larger particle size to match the large AAE measured for the droplet mode BrC aerosol. These are $k_{(467)} = 0.026 \pm 0.001$, $k_{(530)} = 0.017 \pm 0.001$, $k_{(660)} = 0.014 \pm 0.001$, and $n_{467} = 1.47 \pm 0.01$ (Sect.3.4). This finding emphasizes that BrC properties depend on both aerosol size distribution and chemical composition (i.e. an aerosol showing AAE from 2.5 to 6, having high "droplet" mode PC scores. The dependence of this "brown" aerosol on, $m(\lambda)$).

Figure 2 investigates the link between chemical, microphysical, and optical properties. AAE is plotted against PM₁ major constituents, and relevant ratios, is illustrated in Fig. 2 and Fig. 3, where the brown aerosol formation is indicated by the combined increase of AAE (y-axis) and droplet mode PC chemical components (OA, BC, nitrate, and sulfates PM₁ mass fractions, f_x). Grey markers show the longest available time series for AAE and f_x , while coloured markers show the (shorter) time series including the droplet mode aerosol score (marker color). This "brown" aerosol formation depends on the organic mass fraction (f_{OA} , Fig.2a), and is inversely correlated to the mass fractions of BC (f_{BC} , Fig.2b), and sulfate (f_{SO_4} , Fig.2c). The dependence on the nitrate mass fraction (f_{NO_3} , Fig.2d) is not obvious, as high AAE values colour and droplet mode scores are observed for both $f_{NO_3} < d_{med(S)}$ (marker size) (see Sect.3). BrC particles (i.e. particles with AAE >2.3) shows higher f_{NO_3} and lower f_{BC} values coupled to larger $d_{med(S)}$ and high droplet mode aerosol scores. Average values corresponding to BrC aerosol population are as follows (mean \pm standard deviation): AAE = 3.2 ± 0.9 , $f_{NO_3} = 0.38 \pm 0.05$, $f_{BC} = 0.01 \pm 0.01$, $f_{OA} = 0.35 \pm 0.04$ and $f_{NO_3} \approx 0.25$, $f_{SO_4} = 0.1 \pm 0.02$, and $SSA_{530} = 0.98 \pm 0.01$ (and $\sigma_{a467} = 7.6 \pm 3.33 Mm^{-1}$, $\sigma_{s467} = 312 \pm 64 Mm^{-1}$, and SAE = 0.5 ± 0.4).

The relation between this "brown" aerosol and the BC-to-OA ratio (or its inverse OA-to-BC ratio) = Both Fig.2 and Tab.1 show that there is no direct correlation between AAE and f_{OA} . AAE correlates with larger particles (larger $d_{med(S)}$) in the droplet mode (larger PC3 scores), while the f_{OA} / f_{BC} is shown in Fig.3. Uncertainties of AAE, and BC-to-OA in Fig. 3 were calculated propagating uncertainties of PSAP-derived σ_a (Sect.2.2), BC derived by the AAE_{BC} attribution method (Sect.3.1), and AMS-derived OA (Sect.2.3). The area showing the brown aerosol (AAE from 2.5 to 6.6, positive droplet mode PC scores) has high OA-to-BC ratios (note correlation $r = 0.78$ correlates with smaller particles (lower $d_{med(S)}$) from residential heating emissions (larger PC2 scores). There is, however, a significant correlation between AAE and OA-to-BC ratio, Table 470 the ratio of OA to BC ($r = 0.78$, $p < 0.001$). The inverse dependence between this "brown" aerosol formation and the BC-to-OA ratio confirms results of the statistical analysis (correlations with f_{44} and f_{43}) indicating that the brown aerosol is an aged OA. Indeed, it is typical that BC contribution

declines, and OA contribution increases, as the smoke aerosol ages in the atmosphere. Relative proportions of BC and OA in the AAE vs OA-to-BC ratio indicates either combustion characteristics (higher for biofuels than for fossil fuel combustion) or aerosol ageing (lower for fresh aerosols) (Saleh et al., 2014; Bond et al., 2013). The relation between AAE and BC-to-OA relation are indicated in the supplementary material. It is shown that the increase in AAE with decreasing the ratios is illustrated in Figure 3 (light-grey markers show the longest available time series for AAE and BC-to-OA ratio is not simply due to the decreased contribution of BC. The AAE of the aerosol, while coloured markers show the time series including the droplet mode aerosol score and the f_{NO_3}). When the bulk aerosol is dominated by the BrC droplet mode particles, the AAE is indeed dictated by the relative contribution of the OA and BC components. There is a small trend of the lowest AAE values toward 1.5, rather than 1. We explain this if we first consider that the variability from greater than 2.3 ± 1 to 1.5 of AAE is within the uncertainty of the instrumentation. And second, if we consider that these low AAE values are at OA values larger than zero (Suppl. material), similarly to previous results (Lack et al., 2008). The AAE larger than (median \pm uncertainty), and BC-to-OA ratios are lower than 0.05 ± 0.03 . In the inner panel of Fig.3, we parametrize the relation between AAE and BC-to-OA ratios for the bulk aerosol ($AAE = -0.5 \cdot \ln(BCtoOA) + 1$) can hence be due to any spectrally light absorbing material that the AMS could not detect (refractory material, or material in particles smaller than 100 nm and larger than $1 \mu m$), which is consistent with Lu et al. (2015) (this consistency will be analysed in Sect.4.3). When the BrC droplet mode particles dominate the bulk aerosol (black markers in the inner panel of Fig.3, corresponding to PC3 scores > 0), the relation between AAE and BC-to-OA is far stronger ($r = -0.86$, $p < 0.001$). This result highlights the significant dependence of BrC on BC-to-OA ratios in the ambient aerosol.

Taken together, findings finally suggest that the "brown" aerosol type observed in the Po Valley, is secondary in origin and contains aged OA in "droplet" mode particles these findings prove that BrC in the observed ambient aerosol shows $AAE_{467-660} = 3.2 \pm 0.9$ with $k_{(530)} = 0.017 \pm 0.001$, and occurs in particles in the droplet mode size range, enriched in nitrate and poor in BC, with a strong dependance on OA-to-BC ratios, SSA_{530} being 0.98 ± 0.01 .

4.2 A case study

We present here a case study to visualize main aerosol (Figure 4) to show the main microphysical and chemical features of the "brown" BrC aerosol observed. The values of this case study were indicated in Fig.3 by "*": they represent the highest values of AAE, and droplet mode PC scores observed, and thus a case of brown aerosol formation. Figure 4 (panels a, b, c) compares mean values of volume and mass size distributions measured over the whole field experiment with relevant values measured during this case study (first of February

On the case study day (i.e., February 1st, 2013 from 17:30 to 19:00). Relative humidity (RH), the relative humidity was high ($97.5 \pm 0.4\%$, against a mean value for the winter/Winter campaign

of $82 \pm 14 \%$, and a maximum of 98%), temperature averaged $2.8 \pm 0.0 \text{ }^\circ\text{C}$ (campaign mean value= $3.5 \pm 2.8 \text{ }^\circ\text{C}$). Aerosol vertical profiles from a LD40 ceilometer (, and aerosol liquid water content was above $200 \mu\text{g} \cdot \text{m}^{-3}$ (Gilardoni et al., 2016) . Absorption and scattering coefficients at 530 nm (Fig.1 of the supplementary material) ranged from 5 to 10 Mm^{-1} (with larger AAE), and from 300 to 400 Mm^{-1} (with lower Scattering Angstrom Exponents, SAE) respectively, with $\text{SSA}_{530}=0.98 \pm 0.01$. The number concentration of $2\text{-}10 \mu\text{m}$ particles (Fig.4d) indicate a foggy day, except for the middle e) had a peak at approx. $4:00 \text{ a.m. UTC}$ (we interpret this as particle growth by water vapor), and then decreased until $9:00 \text{ a.m. UTC}$. After this, the number concentration of $0.3\text{-}1 \mu\text{m}$ particles increased. This increase occurred just after the part of the day (from $11:00$ to $15 \text{ a.m. to } 2:00 \text{ p.m}$) when the fog layer is shown to dissipate. The day started with low concentrations of sub-micrometer aerosol particles (strong signal in the aerosol vertical profile at the ground (the darker red layer in Fig. 4e) . Coarse mode aerosol particles increased in the early hours of the day, and then decreased, followed by d) is observed to dissipate (we interpret this as droplet evaporation). These processes are consistent with the formation of the droplet mode aerosol (John, 1990; Meng and Seinfeld, 1994; Seinfeld and Pandis, 2006) . the increase of the droplet mode aerosol particles (as indicated by the area in Fig. 4e corresponding to diameters ranging from 500 to 800 nm , and scores (PC3scores – not shown here). We interpret this as formation of fog drops, followed by droplet evaporation, and aerosol droplet mode formation, a plausible mechanism for formation of this aerosol type (John, 1990; Meng and Seinfeld, 1994; Seinfeld and Pandis, 2006) . AAE (Fig.4f)) observed in the afternoon. The case study was selected during this period (1.5 hour from $5:30$ to $7:00 \text{ p.m}$), and relevant data are shown in Fig.2, Fig.3, Fig.5, and Fig.1 of the supplementary material.

During the case study (i.e., from $5:30$ to $7:00 \text{ p.m}$ on February 1^{st} , 2013) we observed peculiar data. AAE was significantly higher than its mean value (up to more than 6 – unfortunately no data is available before $15:00$). Relevant volume ($3.4\text{-}5.3$) than the median value (2.0 ± 0.5 during both field campaigns, and 2.1 ± 0.6 in the Winter). Volume size distribution (Fig. 4a) is centered was narrow and monomodal, centred on the droplet mode (d_m from 450 to 700 nm), the peak being more than four times as high as that of the mean value. Mass. Relevant mass size distributions of the main constituents of nr-PM_{10} (NO_3 , organics, OA, and NH_4) are centered around 700 nm of the vacuum aerodynamic diameter (d_{va}) . Note that $d_{va} = 700 \text{ nm}$ corresponds to $d_m = 468 \text{ nm}$ corresponding to about 500 nm in mobility diameter (for spherical particles with $\rho_p = 1.5 \text{ g} \cdot \text{cm}^{-3}$ in the continuum regime , as d_m and d_{va} are linked by Eq.4 (Seinfeld and Pandis, 2006) :

$$d_{va} = d_m \frac{\rho_p}{\rho_0}.$$

with $\rho_p = 1.4 \text{ g} \cdot \text{cm}^{-3}$ (Seinfeld and Pandis, 2006)). In addition, the organic aerosol OA mass below $d_{va} = 300 \text{ nm}$ was significantly lower than that of the droplet mode, especially when compared to the average field results (Fig. 4c). Relevant absorption and scattering coefficients (not shown here) ranged from 5 to 10 Mm^{-1} , and from 300 to 400 Mm^{-1} , respectively. As shown by this case

545 study, a general feature of the whole field campaign was that the brown aerosol formed in the early
afternoon. It is important to note that the collection efficiency of the HR-ToF-AMS is 50% for 600
nm particles and decreases for larger sizes (Liu et al., 2007). This explains the difference between
the size distributions in fig. Fig. 4a and Fig. 4b at larger sizes.

550 At the light of source apportionment study performed on organic aerosol (Gilardoni et al., 2016) we
explain the increase of AAE during the case study period with the formation of secondary organic
aerosol in the aqueous phase associated with aerosol particles. The analysis of microphysical properties
reported in this study confirms that the aqueous secondary organic aerosol formation adds mass to
the atmospheric aerosol in the droplet mode range. This case study both illustrates and confirms
general features observed for BrC during the whole field campaign.

555 4.3 Discussion in comparison with previous works

In this section we discuss our findings and explore their consistency with literature.

5 Discussion in comparison with previous works

In this section, we discuss findings to explore consistency with literature, and put results in a broader
perspective.

560 The analysis of chemical and microphysical properties shows that BrC associated with the formation
of secondary aerosol has a narrow monomodal size distribution centered around the droplet mode
(400–700 nm) in the entire PM_{10} size range. This result agrees with the observations reported
by Lin et al. (2010), showing that 80% of the mass of atmospheric humic-like substances, a light
absorbing organic aerosol component, was found in the droplet mode. The correspondence between
565 BrC and the droplet mode aerosol points to the important role that aqueous reactions within aerosol
particles can play in the formation of light absorbing organic aerosol (Ervens et al., 2011; Laskin et al., 2015).

4.1 "Brown" aerosol in the ambient atmosphere

570 In Figure 5, relations illustrated in Fig. 2 and Fig. 3 between AAE, f_{OA} , and $f_{OA}/f_{BC} = OA\text{-to-}BC$,
are compared to literature. Our results (obtained in urban ambient air) are compared to previous
findings obtained under "diluted" urban conditions (airborne, and AERONET columnar observations)
(Shinozuka et al., 2009; Russell et al., 2010), or in combustion chambers experiments (Saleh et al., 2014; Lu et al., 2015).

575 Figure 5a shows the relation between AAE (y axis), f_{OA} (x axis), SSA (at 530 nm, marker color),
and $d_{med(S)}$ (marker size). The Pearson's correlation coefficient (r) is 0.56. Fig. 6a is intended to
compare to Russell et al. (2010)'s results, indicated by the black line, and Shinozuka et al. (2009)'s
results, indicated by grey lines. Note that grey lines by Shinozuka et al. (2009) refer to the SSA bins

of 0.90-0.92, 0.96-0.98. The study of optical and 0.98-1.00. There are broad similarities between the three results. As in Russell et al. (2010)'s and Shinozuka et al. (2009)'s work, our data make
 580 evident that increasing f_{OA} values are accompanied by increasing AAE values, when dust is absent. However, there are conditions when AAE increases irrespective of f_{OA} . In contrast, when f_{OA} is normalised to f_{BC} ($f_{OA}/$ chemical properties indicates that the larger AAE values associated with BrC depend on organic fraction in a different way from that in literature (Shinozuka et al., 2009; Russell et al., 2010; Arola et al., 2011). In Figure 5a we compare our measurements collected at the urban background site of Bologna with
 585 the trend expected based on airborne and sunphotometers observations (Shinozuka et al., 2009; Russell et al., 2010). AAE is plotted versus the mass fraction of organic aerosol (f_{BC-OA}), marker colour being SSA_{530} as in Shinozuka et al. (2009)'s Fig.7. We show the best fit lines (thin black lines) identified by Shinozuka et al. (2009) and corresponding to different SSA bins, and the best fit reported by Russell et al. (2010) (thick black line). Note that the larger AAE values in our study (associated to BrC in the droplet mode)
 590 correspond to Shinozuka et al. (2009)'s fit line at $SSA=OA$ -to- BC ratio), there is a strong correlation with AAE ($r=0.78$, Fig. 5b). The increasing OA-to-BC ratio is accompanied by a uniform increase of AAE. As well, there is a weak increase of SSA ($r=0.56$), and $d_{med(S)}$ ($r=0.49$). As in Shinozuka et al. (2009)'s results for SSA bins 0.98-1.00, it is shown that values of $AAE > 3.5$ are at $SSA > 0.98$ (Fig. 6a). Note values measured during -1, but were associated to lower scattering
 595 coefficients in those previous studies. There is consistency between our study and those reported previously. However, our data show that increasing AAE is accompanied by increasing the organic aerosol normalized to BC (Fig.5b, $r=0.78$, $p<0.001$), rather than by increasing organic aerosol (Fig.5a). This comparison adds to the case study (Fig. 5) indicated by "*". All of them are at these high AAEs. This comparison ultimately shows (i) consistency of "brown" aerosol properties
 600 observed from airborne/AERONET, and measured in situ at the ground; (ii) literature that for the ambient aerosol in the lower troposphere AAE correlates with OA-to-BC ratio to be a better indicator than f_{OA} of "brown" aerosol and its large AAE values. ratios far more than with the organic fraction.

Saleh et al. (2014) used the inverse of OA-to-BC to parametrize the AAE of biomass burning
 605 emissions in a combustion chamber experiment. To compare to Saleh et al. (2014)'s and Lu et al. (2015)'s work, panel e of Fig.6 shows AAE versus BC -to- OA (the inverse in log scale of the x axis in Fig. 5b). Black and grey lines in Fig.6c indicate Saleh et al. (2014)'s and Lu et al. (2015)'s least square fit, respectively. There are similar patterns. Both Saleh et al. (2014) and Lu et al. (2015) concluded that this dependence of AAE on the ratios below 0.05 ± 0.03 . Finally,
 610 Fig.5c shows the dependence of AAE on the BC -to- OA ratio can be observed solely for biomass burning OA, and not for fossil fuel OA. Note that we compare, in Fig.5c, different AAE values. In our work, AAE values are due to the whole dust-free aerosol, thus depending on both BC and OA ($AAE_{BC,OA}$). AAE values of Saleh et al. (2014) and Lu et al. (2015) (AAE_{OA}) come from the wavelength-dependence of OA alone (w_{OA}), excluding contributions from BC (AAE_{OA} values are

615 calculated from w_{OA} based on the relation $AAE=w+1$, valid for small particles in the visible range).
The comparison in Fig.5c is thus intended to compare patterns only, not absolute values. In the
Supplementary material, AAE_{BC} is plotted together with $AAE_{BC,OA}$, in the AAE vs BC-to-OA
plot. This figure is intended to indicate wavelength dependence of OA absorption, and suggest
possible AAE_{OA} patterns, increasing with decreasing BC-to-OA, similarly to what observed by
620 Saleh et al. (2014) and Lu et al. (2015).

This comparison strengthens our findings indicating that ratio, as parametrized by Saleh et al. (2014) and
Lu et al. (2015) for biomass burning emissions and primary organic aerosol emissions. The best
fit line to measurements performed in this study (grey line) is similar to the "brown" aerosol (i)
represents an aerosol aged in the atmosphere, and (ii) is not a freshly emitted aerosol fitting lines
625 reported previously (thicker and thinner black lines, showing respectively Saleh et al. (2014)'s and
Lu et al. (2015)'s data). While we cannot compare absolute values because we compare AAE of
the bulk aerosol (this study) to AAE of OA only (Saleh et al., 2014; Lu et al., 2015), it is evident
that patterns are similar. This comparison extends the dependence of AAE on BC-to-OA observed
in chamber experiments (solely for fresh biomass burning primary OA, and not for fossil fuel OA)
630 by Saleh et al. (2014) and Lu et al. (2015) to ambient aerosol dominated by wood burning emissions
(Gilardoni et al., 2016).

as it is not observed in a combustion chamber experiment. If Saleh et al. (2014)'s results are
confirmed, this comparison suggests that this brown aerosol derives from the processing of biomass
burning OA. It is worth noting that the AAE of this secondary "brown" aerosol would probably be
635 higher than that of the fresh biomass burning OA it likely derives from. Lu et al. (2015)'s experiments
similarly suggested that atmospheric processing should not decrease biomass burning OA absorptive
properties.

4.1 Spectral optical properties of the "brown" aerosol

Cluster analysis of aerosol spectral optical properties is becoming more and more used to infer
640 information on aerosol type from optical data (e. g., Bergstrom et al., 2007; Clarke et al., 2007;
Yang et al., 2009; Russell et al., 2010; Gyawali et al., 2012; Lee et al., 2012; Costabile 2013).
This analysis holds promise for future aerosol classification from remote optical measurements
(e.g., AERONET, satellite). Costabile et al. (2013) assessed spectral optical properties of key aerosol
populations through Mie theory: soot, biomass burning, two types of organics, dust and marine
645 particles were simulated through a sectional approach where each of these aerosol types was given a
monomodal PNSD and a set of three refractive indices (RIs) in the visible range. Relevant Ångström
Exponents of extinction, scattering, and absorption (EAE, SAE, AAE), SSA and its spectral variation
(dSSA) were calculated. It was proved that these aerosol types separately cluster within a "paradigm"
where SAE is on the y-axis, dSSA times AAE is on the x-axis, and SSA is on the z-axis (Fig. ??).

650 In this section, we show that experimental data of the "brown" aerosol do cluster in this paradigm,
as well (Fig. ??), and that the cluster of "brown" aerosol data is separated from all other simulated
aerosol types, except that named "large organics". Data of "large organics" and "brown" aerosol do
overlap, indicating that they may represent the same aerosol type. In fact, microphysical properties
of the aerosol type named "large organics" were simulated to be same as those of the droplet mode
655 aerosol (i.e., PNSD peaking in the "large" accumulation mode, 300-800 nm size range). Spectral
optical properties of this "large organics" aerosol type were simulated by RIs of spectrally absorbing
organic material in the visible region: these RIs, given the broad similarities in Fig. ??, can be
assumed to be those of the "brown" aerosol.

This comparison ultimately allows to infer spectral optical properties of "brown" aerosol (Table ??),
660 definitely not a purely scattering component. It is worth noting that the value of k_{530} assumed for the
"brown" aerosol is consistent with literature k_{530} values recently reviewed by Lu et al. (2015) for
the bulk OA obtained from chemically aged primary aerosol. Supplementary material shows the
variability of relevant spectral optical properties with varying mass fractions of PM_{10} major components

4.1 A SOA type "brown" aerosol

665 Findings indicate a relation linking the "brown" aerosol to the aged OA. AMS measurements enable
to map OA ageing level by combining f_{43} and f_{44} (Sect. ??, and Table 1), representing intensities
of the two oxygen-containing ions dominating the OA spectra (see review by Moise et al., 2015). f_{44}
has been found to originate from the dissociation in the AMS of oxidised organic molecules (the
 CO_2^+ fragment from carboxylic acid groups). f_{43} has been related to non-acid oxidised species
670 (the $C_2H_3O^+$ fragment from aldehydes and ketones), in addition to saturated hydrocarbons (the
 $C_3H_7^+$ fragment). Figure ?? shows f_{44} plotted against f_{43} , and their relation with the brown aerosol
(AAE is data color, the droplet mode PC score is data size). This figure is intended to reproduce the
"triangle plot" proposed by ??, which encompasses the majority of OA values measured in ambient
samples. It is showed that the "brown" aerosol (the largest yellow-to-red markers) lies in the oxidised
675 OA region, where most of the semi-volatile oxidised OA measurements taken at the ground lie
(??). The composition found for this "brown" aerosol (high OA, nitrates being a likely component)
, its formation process (involving aqueous phase reactions), and AAEs values, are all coherent
with previous studies, which showed increased light absorption towards UV for SOA particles
(Jacobson, 1999; Lee et al., 2013; Song et al., 2013; Zhang et al., 2013; Powelson et al., 2014; Lin et al., 2014; Laskin et al., 2015)
680 and sources, composition, and AAE of light-absorbing soluble organic aerosol in urban areas (Zhang et al., 2013, 2011).

This comparison reinforces our hypothesis that the "brown" aerosol is an aged OA.

5 Summary and conclusions

We characterized the nondust aerosol having the strongest spectral dependence of light absorption (as indicated by the Absorption Ångström Exponent, AAE) at visible wavelengths investigated optical-chemical-microphysical properties of brown carbon (BrC) in the urban ambient atmosphere of the Po Valley (Bologna). We defined "brown" this bulk aerosol with brown color (it does not necessarily equate to brown carbon). In situ ground ambient measurements of chemical (HR-ToF-AMS), optical (3- λ nephelometer and PSAP), and micro-physical-microphysical (SMPS and APS) aerosol properties were taken carried out in the Po Valley (Bologna), together with ancillary observations.

Findings prove that the observed "brown" aerosol is a secondary aerosol dominated by accumulation mode particles containing organic aerosol (OA).

Conditions when "brown" aerosol dominates the bulk dust-free aerosol were first identified based on AAE values. "Brown" aerosol sources in the urban atmosphere were then investigated by relating these AAE-BrC was identified and characterized by linking its wavelength dependence of light absorption (as indicated by the Absorption Ångström Exponent, AAE) in the visible region to key aerosol populations statistically identified. Physico-chemical properties of this aerosol were characterised: number and mass size distribution, types with known size distributions, and to major PM₁ chemical components (BC, organics OA, nitrate, ammonium, and sulfate); their mass fractions; and relevant ratios (including the BC-to-OA ratio). A case study was illustrated. Overall, the "brown" aerosol has AAE values from 2.5 to 6, is secondary in origin, formed by the larger accumulation mode particles referred to in literature as droplet mode particles, and contains large concentrations of organic aerosol (OA), its OA-to-BC ratio being higher. Nitrate is an additional likely component. BrC measurements were interpreted through numerical simulations (Mie theory) of AAE(d_p, λ, m) resolved by particle size (d_p) and wavelength (λ) dependent complex refractive index ($m_{(\lambda)} = n_{(\lambda)} - ik_{(\lambda)}$) in the visible region.

To our knowledge, no previous work has considered these issues in the ambient atmosphere. This is the first experimental evidence that extends observations by Saleh et al. (2014) to ambient conditions, and provides a micro-physical characterization of this "brown" aerosol. We found that:

(1) AAE increases with increasing the (optically relevant) aerosol size. Larger AAEs (3.2 ± 0.9 , with values up to 5.5) occur when the bulk aerosol size distribution is dominated by the droplet mode, i.e. the large accumulation mode originating from the processing in the aqueous phase. These values identify BrC.

(2) Peculiar $m_{(\lambda)}$ values are necessary in addition to larger particle size to match the high AAE measured for BrC. These $m_{(\lambda)}$ values are theoretically expected to be: $k_{(467)} = 0.026 \pm 0.001$, $k_{(530)} = 0.017 \pm 0.001$, and freshly emitted aerosols (combustion chamber experiments). We found a dependence of AAE on OA similar to what found for airborne and AERONET data, and a dependence of AAE on the BC-to-OA ratio similar to what found for freshly emitted aerosols. Our study adds

720 ~~to these previous studies that: (i) AAE depends on $k_{(660)} = 0.014 \pm 0.001$, and $n_{467} = 1.47 \pm 0.01$ ($SSA_{530} = 0.98 \pm 0.01$), consistent to literature $m_{(\lambda)}$ values for BrC in the ambient atmosphere.~~
~~(3) AAE increases with increasing the OA-to-BC ratio more than on OA, rather than with increasing f_{OA} , the larger AAEs (and thus BrC) corresponding to larger nitrate ($f_{NO_3} = 0.38 \pm 0.05$) and (ii) the link between AAE and lower BC ($f_{BC} = 0.01 \pm 0.01$).~~
~~Consistency of findings with literature was then explored. We compared our results with previous~~
 725 ~~findings obtained for "diluted" urban aerosols (airborne and AERONET observations)~~
~~When exploring consistency of these findings with the literature, our study:~~
~~(i) provides experimental evidence that the size distribution of BrC associated with the formation of secondary aerosol is dominated by the droplet mode, consistent with recent findings pointing to the OA-to-BC (already observed for the freshly emitted primary aerosol from biomass burning) is~~
 730 ~~observed in the ambient atmosphere, as well, where it can be used to identify the "brown" aerosol role of aqueous reactions within aerosol particles in the formation of BrC;~~
~~(ii) adds to sunphotometric observations (e.g., AERONET) that in the lower troposphere AAE correlates with the organic aerosol normalized to BC (i.e., OA-to-BC) far more than with the organic fraction;~~
 735 ~~(iii) extends to the ambient aerosol dominated by wood burning emissions the dependence of AAE on BC-to-OA previously observed in combustion chamber experiments. Finally, the comparison with a simulation work allowed to obtain the following optical signature in the visible region for the "brown" aerosol: AAE of 2.5-6.6, SAE of 0.5-2, SSA of 0.9-1, and average refractive index at 467 nm of 1.460-0.012i.~~
 740 ~~Findings will have important atmospheric implications for modeling studies. These findings are expected to bear important implications for atmospheric modeling studies and remote sensing observations. The link between AAE and the OA-to-BC ratio can be a strong tool to parametrize the "brown" aerosol in the atmosphere, as well as to investigate brown OA and Brown Carbon. It is worth noting that this link Both BrC number size distribution and the dependence of AAE on BC-to-OA~~
 745 ~~can be relevant to parametrize and investigate BrC in the ambient atmosphere. Findings can be used to extrapolate/infer preliminary chemical information from optical ones/information, as optical techniques are increasingly used to characterise aerosol properties.~~

Acknowledgements. This work was realized in the framework of the ~~Supersito Project~~ SUPERSITO Project, financed by the Emilia-Romagna Region (under the DR 1971/13). The work was partly accomplished in the
 750 framework of the DIAPASON ("Desert-dust Impact on Air quality through model-Predictions and Advanced Sensors ObservationS") project, funded by the European Commission (LIFE+ 2010 ENV/IT/391).

References

- [Alexander, D. T., Crozier, P. A., and Anderson, J. R.: Brown carbon spheres in East Asian outflow and their optical properties. *Science*, 321\(5890\), 833-836, 2008.](#)
- 755 Andreae, M. O. and Gelencsér, A.: Black carbon or brown carbon? The nature of light-absorbing carbonaceous aerosols, *Atmos. Chem. Phys.*, 6, 3131-3148, doi:10.5194/acp-6-3131-2006, 2006.
- Arola, A., Schuster, G., Myhre, G., Kazadzis, S., Dey, S., and Tripathi, S. N.: Inferring absorbing organic carbon content from AERONET data, *Atmos. Chem. Phys.*, 11(1), 215-225, 2011.
- Backman, J., Virkkula, A., Vakkari, V., Beukes, J. P., Van Zyl, P. G., Josipovic, M., Piketh, S., Tiitta, P.,
760 Chiloane, K., Petäjä, T., Kulmala, M., and Laakso, L.: Differences in aerosol absorption Ångström exponents between correction algorithms for a particle soot absorption photometer measured on the South African Highveld, *Atmos. Meas. Tech.*, 7, 4285-4298, doi:10.5194/amt-7-4285-2014, 2014.
- Bahadur, E., Praveen, P. S., Xu, Y., and Ramanathan, V.: Solar absorption by elemental and brown carbon determined from spectral observations, *P. Natl. A. Sci.*, 109, 17366-17371, 2012.
- 765 Bellouin, N.: Aerosols: The colour of smoke, *Nat. Geosci.*, 7(9), 619-620, 2014.
- Bergstrom, R. W., Russell, P. B., and Hignett, P.: Wavelength Dependence of the Absorption of Black Carbon Particles: Predictions and Results from the TARFOX Ex Atmos. Chem. Phys., 13, 10535-10543, ~~2013~~-2002.
- [Bohren, C. F., and D. R. Huffman, 1983: Absorption and Scattering of Light by Small Particles. John Wiley, 232 pp.](#)
- 770 Bond, T. C., Anderson, T. L., and Campbell, D.: Calibration and intercomparison of filter-based measurements of visible light absorption by aerosols, *Aerosol Sci. Tech.*, 30, 582-600, 1999.
- [Bond, T. C., Bergstrom, R. W.: Light absorption by carbonaceous particles: An investigative review. *Aerosol Sci. Tech.*, 40\(1\), 27-67, 2006.](#)
- 775 Bond, T.C., Doherty, S.J., Fahey, D.W., Forster, P. M., Berntsen, T., DeAngelo, B.J., Flanner, M.G., Ghan, S., Kärcher, B., Koch, D., Kinne, S., Kondo, Y., Quinn, P.K., Sarofim, M.C., Schultz, M.G., Schulz, M., Venkataraman, C., Zhang, H., Zhang, S., Bellouin, N., Guttikunda, S. K., Hopke, P. K., Jacobson, M. Z., Kaiser, J. W., Klimont, Z., Lohmann, U., Schwarz, J. P., Shindell, D., Storelvmo, T., Warren, S.G., Zender, C.S.: Bounding the role of black carbon in the climate system: A scientific assessment, *J. Geophys. Res.*
780 *Atmos.*, 118, 5380-5552, doi:10.1002/jgrd.50171, 2013.
- [Brines, M. and Dall'Osto, M. and Beddows, D. C. S. and Harrison, R. M. and Gómez-Moreno, F. and Núñez, L. and Artíñano, B. and Costabile, F. and Gobbi, G. P. and Salimi, F. and Morawska, L. and Sioutas, C. and Querol, X.: Traffic and nucleation events as main sources of ultrafine particles in high-insolation developed world cities. *Atmos. Chem. Phys.*, 15, 5929-5945, doi:10.5194/acp-15-5929-2015, 2015.](#)
- 785 Cappa, C. D., Lack, D. A., Burkholder, J. B., Ravishankara, A. R.: Bias in filter-based aerosol light absorption measurements due to organic aerosol loading: Evidence from laboratory measurements. *Aerosol Science and Technology Sci. Tech.*, 42(12), 1022-1032, 2008.
- Costabile, F., Birmili, W., Klose, S., Tuch, T., Wehner, B., Wiedensohler, A., Franck, U., König, K., and Sonntag, A.: Spatio-temporal variability and principal components of the particle number size distribution in an
790 urban atmosphere, *Atmos. Chem. Phys.*, 9, 3163-3195, doi:10.5194/acp-9-3163-2009, 2009.

Costabile, F., Barnaba, F., Angelini, F., and Gobbi, G. P.: Identification of key aerosol populations through their size and composition resolved spectral scattering and absorption, *Atmos. Chem. Phys.*, 13, 2455-2470, doi:10.5194/acp-13-2455-2013, 2013.

~~Costabile, F., Angelini,~~

795 ~~DeCarlo, P. F., Barnaba, F., Gobbi, G.P.: Partitioning of Black Carbon between ultrafine and fine particle modes in an urban airport vs. urban background environment, *Atmos. Environ.*, 102, 136-144, 2015.~~
~~Crippa, M., Canonaco, F., Lanz, V., Trimborn, A., Northway, M., Allan, J.D., Carbone, S., Capes, G., Ceburnis, D., Dall'Osto, M., Day, D. A., DeCarlo, P.F., Ehn, J., Jayne, J. T., Aiken, A. C., Eriksson, A., Freney, E., Hildebrandt-Ruiz, L., Gonin, M., Hillamo, M., Fuhrer, K., Horvath, T., Docherty, K. S., Worsnop, D. R., and Jimenez, J. L.: Field-deployable, high-resolution, time-of-flight aerosol mass spectrometer, *Anal. Chem.*, 78, 8281-8289, 2006.~~

800 ~~D. R., and Jimenez, J. L.: Field-deployable, high-resolution, time-of-flight aerosol mass spectrometer, *Anal. Chem.*, 78, 8281-8289, 2006.~~

~~Ervens, B., Turpin, B. J., and Weber, R. J.: Secondary organic aerosol formation in cloud droplets and aqueous particles (aqSOA): a review of laboratory, field and model studies, *Atmos. Chem. Phys.*, 11, 11069-11102, doi:10.5194/acp-11-11069-2011, 2011.~~

805 ~~doi:10.5194/acp-11-11069-2011, 2011.~~

~~Flowers, B. A., Mensah, A. A., Mohr, C., Nemitz, E., O'Dowd, C., Ovadnevaite, J., Pandis, S. N., Petj, T., Poulain, L., Saarikoski, S., Sellegri, M. K., Swietlicki, E., Tiitta, P., Worsnop, D. R., Baltensperger, U., and PrvSUPERSCRIPTot, A. S. H.: Organic aerosol components derived from 25 AMS data sets across Europe using a consistent ME-2 based source apportionment approach, *Mazzoleni, C., Stone, E. A., Schauer, J. J., Kim, S.-W., and Yoon, S. C.: Optical-chemical-microphysical relationships and closure studies for mixed carbonaceous aerosols observed at Jeju Island; 3-laser photoacoustic spectrometer, particle sizing, and filter analysis, *Atmos. Chem. Phys.*, 14, 6159-6176, 10387-10398, doi:10.5194/acp-14-6159-2014, 2014.*~~

810 ~~and filter analysis, *Atmos. Chem. Phys.*, 14, 6159-6176, 10387-10398, doi:10.5194/acp-14-6159-2014, 2014.~~

~~DeCarlo,~~

815 ~~Gilardoni, S., Massoli, P.F., Kimmel, J.R., Trimborn, A., Northway, M.J., Jayne, J.T., Aiken, A., Paglione, M., Giulianelli, L., Carbone, C., Gonin, Rinaldi, M., Fuhrer, K., Horvath, T., Docherty, K., Decesari, S., Worsnop, D.R., and Jimenez, J.L.: Field-deployable, high-resolution, time-of-flight aerosol mass spectrometer, *Anal. Chem.*, 78, 8281-8289~~

820 ~~Sandrini, S., Costabile, F., 2006.~~
~~Ervens, B., Turpin, B.J., and Weber, R.J.: Secondary organic aerosol formation in cloud droplets and aqueous particles (aqSOA): a review of laboratory, field and model studies, *Atmos. Chem. Phys.* Gobbi, G.P., Pietrogrande, M.C., Visentin, M., 11069-11102, doi:10.5194/acp-11-11069-2011, 2011.~~
~~Scotto, F., Fuzzi, S., Facchini, M.C.: Direct observation of aqueous secondary organic aerosol from biomass burning emissions, *P. Natl. A. Sci.*, 113.36: 10013-10018, 2016.~~

Gyawali, M., Arnott, W. P., Lewis, K., and Moosmüller, H.: In situ aerosol optics in Reno, NV, USA during and after the summer 2008 California wildfires and the influence of absorbing and non-absorbing organic coatings on spectral light absorption, *Atmos. Chem. Phys.*, 9, 8007-8015, doi:10.5194/acp-9-8007-2009, 2009.

825 ~~and after the summer 2008 California wildfires and the influence of absorbing and non-absorbing organic coatings on spectral light absorption, *Atmos. Chem. Phys.*, 9, 8007-8015, doi:10.5194/acp-9-8007-2009, 2009.~~

Hinds W.C., *Aerosol Technology*, 2nd, Edition., Wiley, New York, 1999.

- Khlystov, A., Stanier, C., Pandis, S. N.: An Algorithm for Combining Electrical Mobility and Aerodynamic Size
830 Distributions Data when Measuring Ambient Aerosol, Special Issue of Aerosol Science and Technology on
Findings from the Fine Particulate Matter Supersites Program., *Aerosol Sci. Tech.*, 38, S1, 229-238, 2004.
- Lack, D.A., Cappa, C.D., Covert, D.S., Baynard, T., Massoli, P., Sierau, B., Bates, T.S., Quinn, P.K., Lovejoy,
E.R. and Ravishankara, A.R.: Bias in filter-based aerosol light absorption measurements due to organic
aerosol loading: Evidence from ambient measurements. *Aerosol Science and Technology Sci. Tech.*, 42(12),
835 ~~pp.1033-1041~~[1033-1041](#), 2008.
- Lack, D. A. and Langridge, J. M.: On the attribution of black and brown carbon light absorption using the
Ångström exponent, *Atmos. Chem. Phys.*, 13, 10535-10543, doi:10.5194/acp-13-10535-2013, 2013.
- Laskin, A., Laskin, J., and Nizkorodov, S. A.: Chemistry of Atmospheric Brown Carbon, *Chem. Rev.*, doi:
10.1021/cr5006167, 2015.
- 840 Lee, A.K.Y., Zhao, R., Li, R., Liggio, J., Li, S.-M., Abbatt, J.P.D.: Formation of light absorbing organo-nitrogen
species from evaporation of droplets containing glyoxal and ammonium sulfate, *Environ. Sci. Technol.*, 47
(22), 12819-12826, doi:10.1021/es402687w, 2013.
- [Lin, P., Huang, X.-F., He, L.-Y., Yu, J. Z.: Abundance and size distributions of HULIS in ambient aerosols at a
rural site in South China. *J. Aerosol Sci.*, 41 \(1\), 74–87, 2010.](#)
- 845 Lin, Y.-H., Budisulistiorini, S.H., Chu, K., Siejack, R.A., Zhang, H., Riva, M., Zhang, Z., Gold, A., Kautzman,
K.E., Surratt, J.D.: Light-absorbing oligomer formation in secondary organic aerosol from reactive uptake of
isoprene epoxydiols, *Environ. Sci. Technol.*, 48 (20), 12012-12021, doi: 10.1021/es503142b, 2014.
- [Liu, P. S., Deng, R., Smith, K. A., Williams, L. R., Jayne, J. T., Canagaratna, M. R., Moore, K., Onasch, T.B.,
Worsnop, D.R., Deshler, T. : Transmission efficiency of an aerodynamic focusing lens system: Comparison
850 of model calculations and laboratory measurements for the Aerodyne Aerosol Mass Spectrometer. *Aerosol
Sci. Tech.*, 41\(8\), 721-733, doi: 10.1080/02786820701422278, 2007.](#)
- Lu, Z., Streets, D.G., Winijkul, E., Yan, F., Chen, Y., Bond, T.C., Feng, Y., Dubey, M.K., Liu, S., Pinto, J.P.,
Carmichael, G.R.: Light absorption properties and radiative effects of primary organic aerosol emissions,
Environ. Sci. Technol., 49 (8), 4868-4877, doi: 10.1021/acs.est.5b00211, 2015.
- 855 Jacobson, M. Z.: Isolating nitrated and aromatic aerosols and nitrated aromatic gases as sources of ultraviolet
light absorption, *J. Geophys. Res. - Atmos.*, 104(D3), 3527-3542, 1999.
- Jimenez, J. L., Jayne, J.T., Shi, Q., Kolb, C.E., Worsnop, D.R., Yourshaw, I., Seinfeld, J.H., Flagan, R.C., Zhang,
X., Smith, K.A. and Morris, J.W.: Ambient aerosol sampling using the Aerodyne Aerosol Mass Spectrometer,
J. Geophys. Res. - Atmos., 108 (D7), 1984-2012, doi:10.1029/2001jd001213, 2003.
- 860 John, W., Wall, S. M., Ondo, J. L., and Winklmayr, W.: Modes in the size distributions of atmospheric inorganic
aerosol, *Atmos. Environ.*, 24A, 2349-2359, 1990.
- Meng, Z. and Seinfeld, J. H.: On the source of the submicrometer droplet mode of urban and regional aerosols,
Aerosol Sci. Tech., 20, 253-265, 1994.
- Middlebrook, A. M., Bahreini, R., Jimenez, J. L. and Canagaratna, M. R.: Evaluation of Composition-
865 Dependent Collection Efficiencies for the Aerodyne Aerosol Mass Spectrometer using Field Data, *Aerosol
Sci. Tech.*, 46, 258-271, doi:10.1080/02786826.2011.620041, 2012.
- Moise, T., Flores, J.M., Rudich, Y.: Optical Properties of Secondary Organic Aerosols and Their Changes by
Chemical Processes, *Chem. Rev.*, 115.10, 4400-4439, doi: 10.1021/cr5005259, 2015.

- Moosmüller, H., Chakrabarty, R. K., Ehlers, K. M., and Arnott, W. P.: Absorption Ångström coefficient, brown
 870 carbon, and aerosols: basic concepts, bulk matter, and spherical particles, *Atmos. Chem. Phys.*, 11, 1217-
 1225, doi:10.5194/acp-11-1217-2011, 2011.
- [Ng, N. L., Canagaratna, M. R., Zhang, Q., Jimenez, J.,
 Pohjola, M. A., Pirjola, L., Tian, J., Ulbrich, I. M., Kroll, J. H., Docherty, K. S., Chhabra, P. S., Bahreini, R.,
 Murphy, S. M., Seinfeld, J. H., Hildebrandt, L., Donahue, N. M., DeCarlo, P. F., Lanz, V., Karppinen, A.,
 875 PrvSUPERSCRIPTot, A. S. H., Dinar, E., Rudich, Y., and Worsnop, D. R.: Organic aerosol components
 observed in Northern Hemispheric datasets from Aerosol Mass Spectrometry, *Atmos. Chem. Phys.*, 10,
 4625-4641, doi:10.5194/acp-10-4625-2010, 2010.](#)
- [Ng, N. L., Canagaratna, M. R., Jimenez, J. L., Chhabra, P. S., Seinfeld, J. H., and Worsnop, D. R.: Changes in
 organic aerosol composition with aging inferred from aerosol mass spectra, et al.: Evaluation and modelling
 880 of the size fractionated aerosol particle number concentration measurements nearby a major road in Helsinki
 - Part I: Modelling results within the LIPIKA project, *Atmos. Chem. Phys.*, 11\(13\), 6465-6474, 2011. 7,
 4065-4080, 2007.](#)
- Pöschl, U.: Aerosol particle analysis: challenges and progress. *Anal. Bioanal. chem.*, 375.1, 30-32, DOI
 10.1007/s00216-002-1611-5, 2003.
- 885 Powelson, M.H., Espelien, B.M., Hawkins, L.N., Galloway, M.M., De Haan, D.O.: Brown carbon formation by
 aqueous-phase carbonyl compound reactions with amines and ammonium sulfate, *Environ. Sci. Technol.*, 48
 (2), 985-993, doi: 10.1021/es4038325, 2014.
- Quinn, P. K., Bates, T. S., Coffman, D. J., and Covert, D. S.: Influence of Particle Size and Chemistry on the
 Cloud Nucleating Properties of Aerosols, *Atmos. Chem. Phys.* 8(4), 1029-1042, 2008.
- 890 Russell, P. B., Bergstrom, R. W., Shinozuka, Y., Clarke, A. D., DeCarlo, P. F., Jimenez, J. L., Livingston, J. M.,
 Redemann, J., Dubovik, O., and Strawa, A.: Absorption Ångström Exponent in AERONET and related data
 as an indicator of aerosol composition, *Atmos. Chem. Phys.*, 10, 1155-1169, doi:10.5194/acp-10-1155-2010,
 2010.
- Saleh, R., Hennigan, C. J., McMeeking, G. R., Chuang, W. K., Robinson, E. S., Coe, H., Donahue, N. M.,
 895 and Robinson, A. L.: Absorptivity of brown carbon in fresh and photo-chemically aged biomass-burning
 emissions, *Atmos. Chem. Phys.*, 13, 7683-7693, doi:10.5194/acp-13-7683-2013, 2013.
- Saleh, R., Robinson, E. S., Tkacik, D. S., Ahern, A. T., Liu, S., Aiken, A. C., Sullivan, R. C., Presto, A. A.,
 Dubey, M. K., Yokelson, R. J., Donahue, N. M., and Robinson, A. L.: Brownness of organics in aerosols
 from biomass burning linked to their black carbon content, *Nat. Geosci.*, 7, 647-650, 2014.
- 900 Seinfeld, J. H. and Pandis, S. P.: *Atmospheric Chemistry and Physics*, 2nd edn., John Wiley, New York, USA,
 1232 pp., 2006.
- Shapiro, E. L., Szprengiel, J., Sareen, N., Jen, C. N., Giordano, M. R., and McNeill, V. F.: Light-absorbing
 secondary organic material formed by glyoxal in aqueous aerosol mimics, *Atmos. Chem. Phys.*, 9, 2289-
 2300, doi:10.5194/acp-9-2289-2009, 2009.
- 905 Shinozuka, Y., Clarke, A. D., DeCarlo, P. F., Jimenez, J. L., Dunlea, E. J., Roberts, G. C., Tomlinson, J. M.,
 Collins, D. R., Howell, S. G., Kapustin, V. N., McNaughton, C. S., and Zhou, J.: Aerosol optical properties
 relevant to regional remote sensing of CCN activity and links to their organic mass fraction: airborne obser-

vations over Central Mexico and the US West Coast during MILAGRO/INTEX-B, *Atmos. Chem. Phys.*, 9, 6727-6742, doi:10.5194/acp-9-6727-2009, 2009.

910 Song, C., Gyawali, M., Zaveri, R.A., Shilling, J.E., Arnott, W.P.: Light absorption by secondary organic aerosol from α -pinene: Effects of oxidants, seed aerosol acidity, and relative humidity, *J. Geophys. Res.*, 118 (20), 11741-11749, doi: 10.1002/jgrd.50767, 2013.

~~Virkkula, A., Ahlquist, N. C., Covert, D. S., Arnott, W. P., Sheridan, P. J., Quinn, P. K., and Coffman, D. J.: Modification, calibration and a field test of an instrument for measuring light absorption by particles, *Aerosol Sci. Tech.*, 39, 68–83, 2005.~~

915 Virkkula, A.: Correction of the calibration of the 3-wavelength Particle Soot Absorption Photometer (3 λ PSAP), *Aerosol Sci. Tech.*, 44, 706–712, 2010.

Zhang, X., Lin, Y. H., Surratt, J. D., Zotter, P., Prévôt, A. S., Weber, R. J.: Light-absorbing soluble organic aerosol in Los Angeles and Atlanta: A contrast in secondary organic aerosol. *Geophys. Res. Lett.*, 38(21),

920 2011.

Zhang, X., Y.-H. Lin, J. D. Surratt, and R. J. Weber: Sources, composition and absorption Ångström exponent of light-absorbing organic components in aerosol extracts from the Los Angeles Basin, *Environ. Sci. Technol.*, 47(8), 3685-3693, 2013.

TABLES

Table 1. Statistically significant ($p < 0.001$) Pearson's correlation coefficients (r) between: Absorption Ångström Exponent (AAE) at 467-660 nm; scores of principal components (PC1-PC4) of particle number size distributions obtained major aerosol types identified by Principal Component Analysis (PCA (PC1 is the road traffic related aerosol, PC2 is the residential heating related aerosol, and PC3 is the droplet mode aerosol); mass concentration and mass fractions (f_x) of Black Carbon (f_{BC}), organics (f_{OA}), nitrate (f_{NO_3}), sulfate (f_{SO_4}), and ammonium (f_{NH_4}); optically relevant aerosol size representative of the entire aerosol population (calculated as median mobility diameter of the particle surface size distribution ($d_{med(S)}$); BC mass concentration (BC); organic aerosol (OA) to BC ratio (OA-to-BC); ratio ratios. See Tab. 1 and Tab. 2 of the AMS signal at m/z 44 and m/z 43 to Supplementary material for all the total organics AMS signal (f_{TO} and f_{43}) relevant values. Note that PC3 is the "droplet" mode PC.

r	AAE	$d_{med(S)}$	BC	f_{BC}	OA	f_{OA}	OA-to-BC
AAE- $d_{med(S)}$	0.60	0.48	-0.26	-0.37	0.56	0.78	-0.31
AAE	0.60	0.31	0.08	0.00	-0.1	-0.35	-0.22
PC3-PC1	0.67	0.60	-0.35	-0.42	0.64	0.60	-0.35
$d_{med(S)}$ -PC2	0.48	-0.52	0.22	-0.48	0.38	0.48	-0.12
PC3	0.66	0.60	real part -0.38	k_λ -0.53	λ 0.12	-0.52	0.54

$1.512 \pm 0.017 \cdot 10^{-3} \pm 0.001660 \text{ nm height}$

925 **FIGURES**

The "droplet" mode of the particle number size distribution (PNSD). Factor loadings calculated by PNSD Principal Component Analysis (PCA) are plotted against electrical mobility particle diameter (d_m). Factor loadings are PCA statistical variables indicating correlations between PNSDs and the droplet mode PCA component. Data from this study (brown line) are compared with data
930 obtained by Costabile et al. (2009) in Leipzig (Germany) at: (a) combined urban sites for 70 days in Spring 2005 (green, blue, red, and black lines, as indicated in the legend), and (b) a single site from long-term (2 years) measurements (black line).

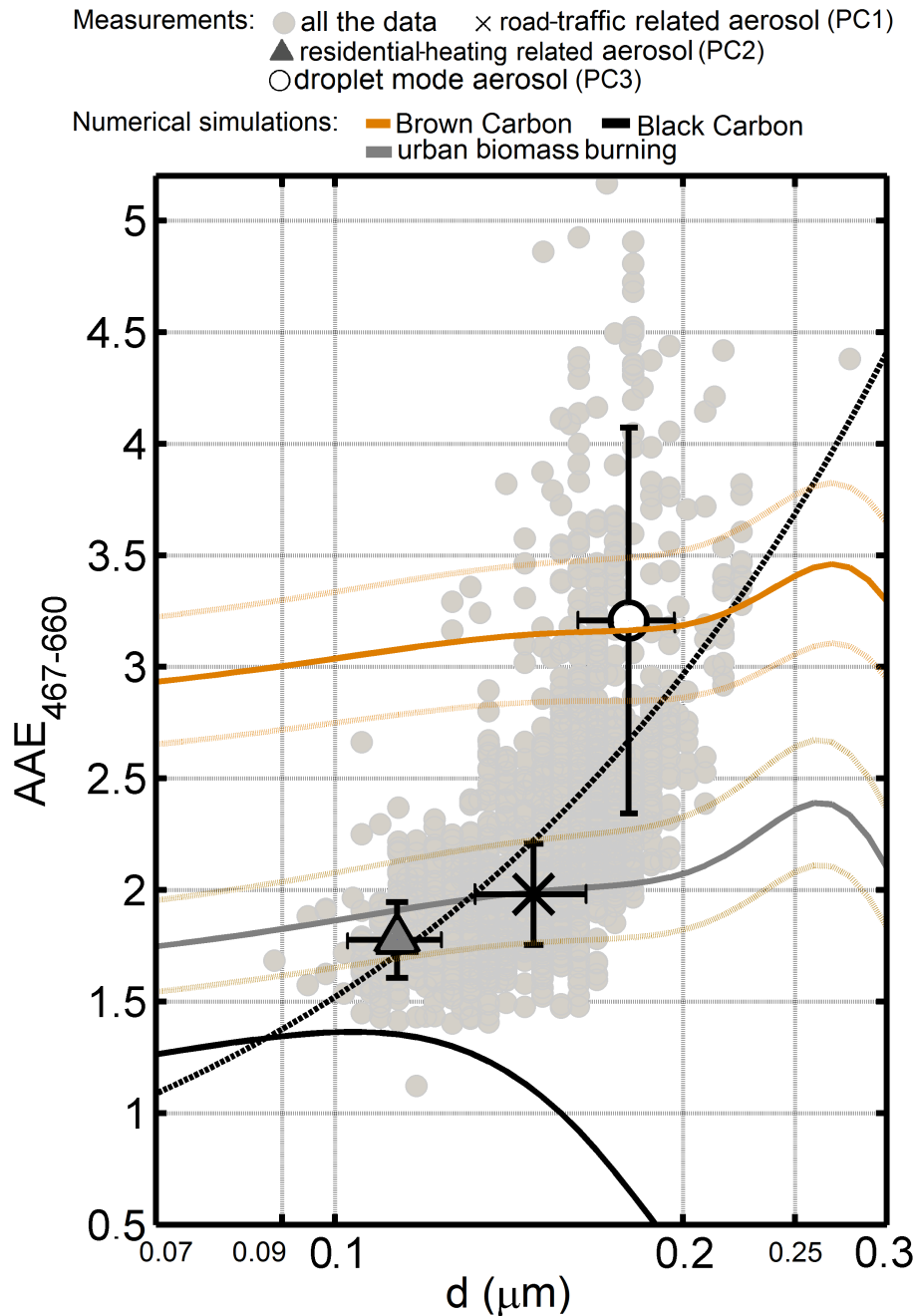


Figure 1. Correlation plot Experimentally measured and numerically simulated (Mie theory) relation between Absorption Ångström Exponent at 467-660 nm (AAE) at 467-660 nm and the "droplet-mode" aerosol size (x-axis-d). For measurements: (i) d is represented by the score-mobility median diameter of the principal component-PM₁₀ particle surface size distribution (PC_{d_{med(S)}}); (ii) all the data measured are indicated by light grey markers, the dotted black line representing the droplet-mode-aerosol best linear fit to these data; (iii) major aerosol types identified (Sect. Data color is the Organic-Aerosol-to-Black-Carbon-ratio-3.3) are indicated by darker markers (OA-to-BC median ± standard deviation). The Pearson's correlation coefficient For numerical simulations (Sect.3.4) is: patterns theoretically expected for BrC, BC, and urban biomass burning are indicated by brown, black and grey thick lines respectively, the dotted thinner lines indicating the uncertainty of the refractive index ($m_{(\lambda)} = n_{(\lambda)} - ik_{(\lambda)}$) set to ±0.01 for $n_{(\lambda)}$ and ±0.001 for $k_{(\lambda)}$.

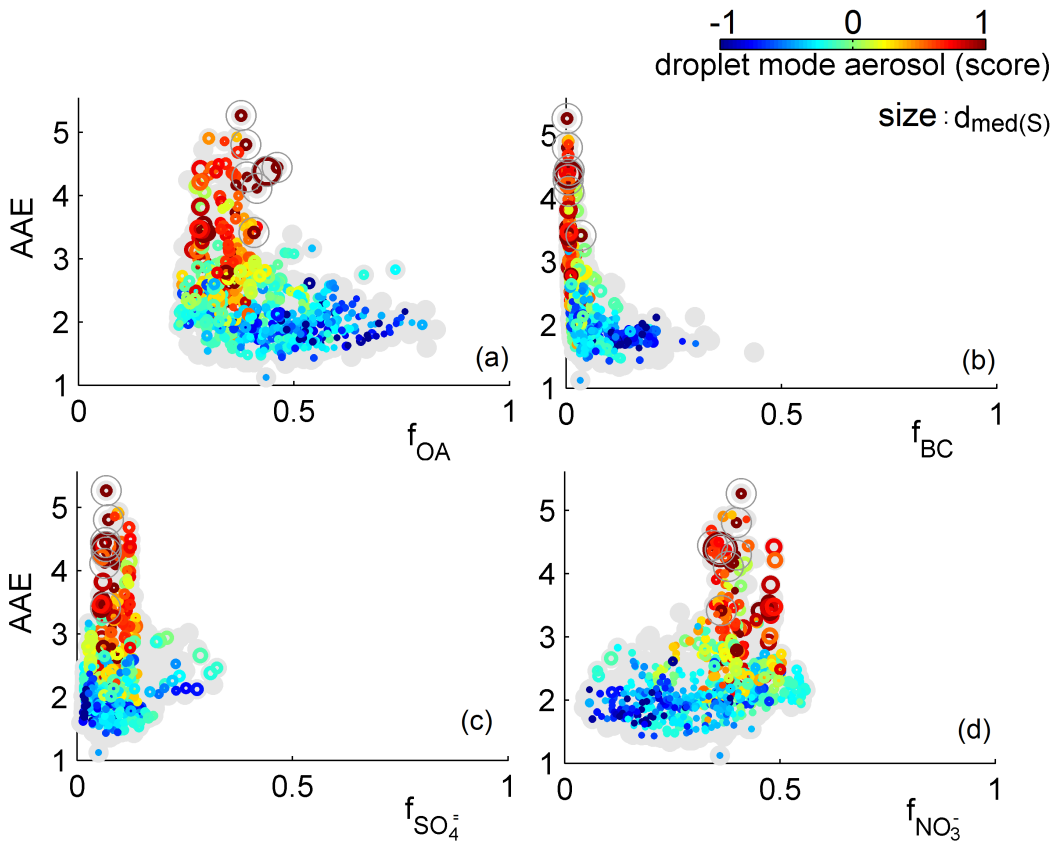


Figure 2. Correlation plots between Physicochemical features of Brown Carbon. Absorption Ångström Exponent at 467-660 nm (AAE) and plotted against mass fractions (f_x) of: (a) organic aerosol (Organic Aerosol (f_{OA})), (b) Black Carbon (f_{BC}), (c) sulfate ($f_{SO_4^-}$), and (d) nitrate ($f_{NO_3^-}$). Grey markers show the longest available time series for AAE and f_x , while marker color and size indicate the score (shorter time series including values) of the droplet mode aerosol. Relevant Pearson's correlation coefficients and aerosol size ($d_{med(S)}$) are, respectively (Sect.3). Data indicated by dark grey "o" show case study values illustrated in Fig. 4.

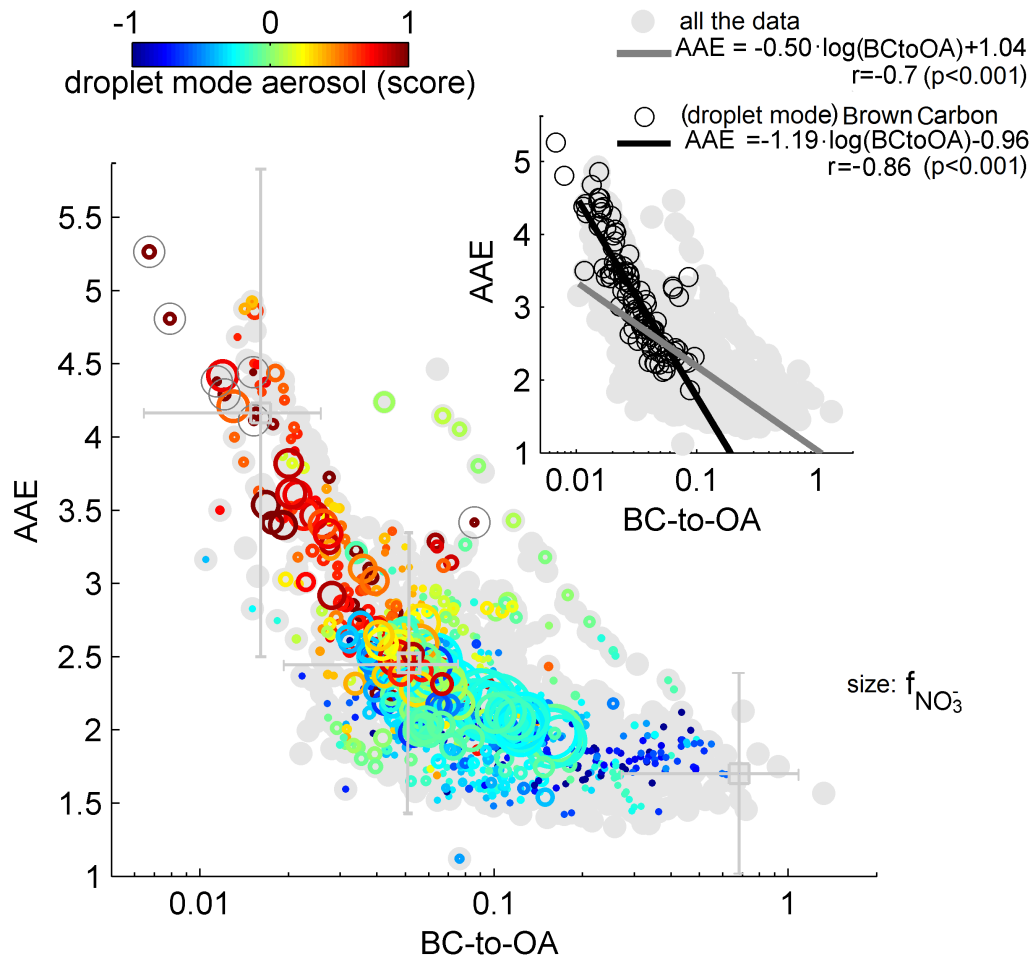


Figure 3. Relation between "brown aerosol" and Black Carbon (BC) to Organic Aerosol (OA) ratio (BC-to-OA) Dependence of AAE on OA-to-BC ratios. Absorption Ångström Exponent Grey markers show the longest available time series for AAE at 467-660 nm (AAE) is plotted against and BC-to-OA. Data, while marker color is and size indicate the score (shorter) time series including relevant values of the droplet mode PC extracted by the statistical analysis aerosol score and nitrate mass fraction, respectively (Sect. Data size is the median diameter of the particle surface size distribution 3). Median values ($d_{med(S)}$) grey squares) and relevant data uncertainty are indicated at the upper, mean, and lower AAE bins. Data indicated by dark grey "*" show case-study values illustrated in Fig. 4. Grey bars indicate measurement uncertainty Inner panel: best fit lines with relevant Eq. and Pearson's correlation coefficients (r, p) to all the data measured (grey line) and droplet mode BrC data (black line) (as indicated by droplet mode aerosol score > 0).

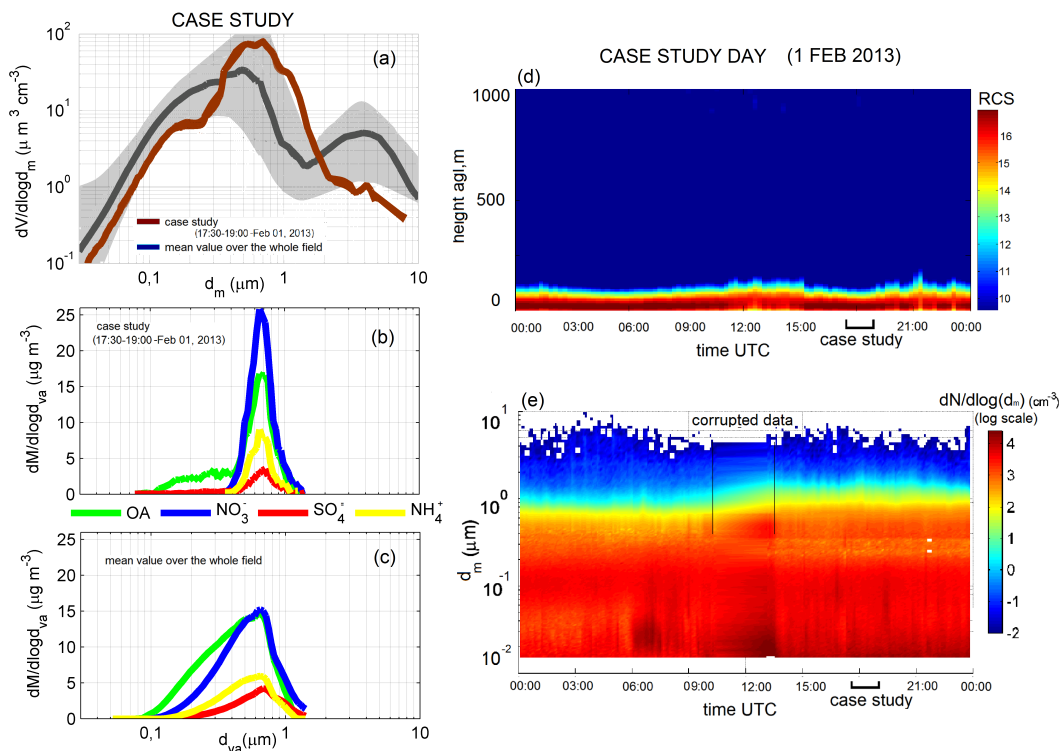


Figure 4. A case-study case study illustrating BrC major features of the "brown aerosol". Case-study Case study time period (1.5 hours) is the first of February, 2013, from 17:30 to 19:00 UTC. Case-study on February 1st, 2013. Case study values are compared with mean values over the whole field experiment. Panels illustrate: (a) particle volume size distribution ($dV/d\log_{10}d_m$, based on electrical mobility particle diameter d_m) during the case-study case study and relevant mean values; (b) particle mass size distribution ($dM/d\log_{10}d_{va}$, based on vacuum aerodynamic diameter, d_{va}) during the case-study case study, and (c) relevant mean values; (d) aerosol vertical profiles in the atmosphere during the case-study entire case study day (time-height cross section of the range corrected signal, $RCS=\ln(S \times R^2)$, from an LD40 ceilometer); (e) particle number size distributions during the case-study day (whiter area includes corrupted data); (f) Absorption Ångström Exponent at 467-660 nm (AAE) during the entire case study day (brown circles), and relevant statistical values during the whole field (grey box-plots, showing median, percentiles, and outliers).

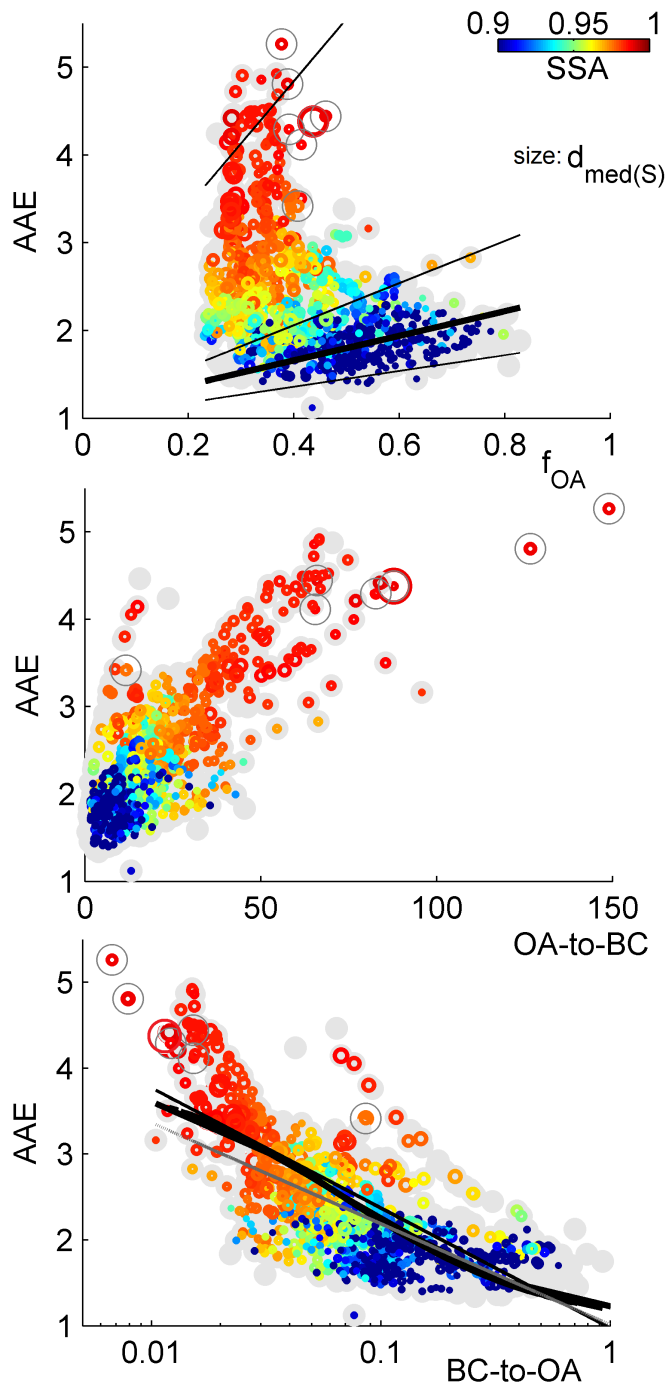


Figure 5. Dependence of Absorption Ångström Exponent at 467-660 nm (AAE) on against: (a) organic aerosol OA mass fraction (f_{OA}), (b) Organic Aerosol (OA) to Black Carbon (BC) ratio (OA-to-BC) ratios, and (c) BC-to-OA ratios. Data color is Single Scattering Albedo. Grey markers show the longest available time series for AAE and f_{OA} , while coloured markers show the (shorter) time series including SSA at 530 nm. Data and aerosol size is median diameter of particle surface size distributions ($d_{med,S}$, ranging from 50 to 300 nm). Data indicated by "*" show case study values illustrated in Fig. 4. Relevant Pearson's correlation coefficients ($r_{Sect.3}$) are indicated. For comparison, we show previous results: Best fit lines taken from: (ai) by Russell et al. (2010) (black line) and Shinozuka et al. (2009) (grey lines, for the at different SSA bins of 0.90-0.92, i.e. 0.98-1.00, 0.96-0.98, 0.90-0.92, from top to bottom), and 0.98-1.00 Russell et al. (2010) are indicated in panel a (thin and thick black lines respectively); (eii) by Saleh et al. (2014) (black line), and Lu et al. (2015) are indicated in panel c (grey line). Note that AAE includes contributions from both BC (black thick